We would like to thank both anonymous referees for their valuable comments on the manuscript which led to a significant improvement of the manuscript. According to the reviewers suggestions we included an additional Figure (now Figure 6). For the specific replys below we refer to the figure numbering of the original version. Referee #1 comments are given in bold, the answers in standard font. Changes to the text are in italics.

General comments:
1) I miss through the paper a clear separation between the role of synoptic and mesoscale in the presentation of the results (section 3). At section 3.1 they described the synoptic situation, but little is mentioned on the potential arrival of anabatic winds characterize with different meteorological and atmospheric composition. I realize that it is difficult to establish a clear difference between the synoptic and mesoscale contribution, but I believe it is necessary to comment the role of mesoscale for a measurement site that is higher than 800 meters.

Indeed the mountainous terrain can influence the regional circulation around the measurement site, resulting in local flow conditions which may have an impact on the diurnal patterns of the tracer measurements. Figure 12 and Figure 13 show the diurnal cycles of CO_2 and O_3 at the surface site. The diurnal cycles are not shifted nor they vanish entirely, which one would expect from advected local "polluted" air from the valleys, if anabatic winds would play a strong role on the studied day. Additionally, during the entire day the wind direction is quite constant which is now shown in the new Figure 6.

2) Key variables like the potential temperature and wind (speed and direction) could be shown and discuss more in depth. The values of the potential temperature inversion are very large (3 and 10 K) for typical boundary layers formed over land. I believe a figure and a more elaborated discussion is needed here.

We included a new Figure 6 with profiles of the virtual potential temperature, wind speed and wind direction from the radio soundings just before and after each flight. We changed the manuscript accordingly:
Figure 6 shows radio sounding profiles of the virtual potential temperature, wind speed and wind direction from the surface up to an altitude of 3200 m before and after the flights on 6 September 2015. [...]. The wind direction within the PBL and FT was mostly constant during that day, whereas the wind speed increased within the FT and decreased within the PBL during the day.
Further discussions are given to reviewer #2.

3) At section 3.2 it is mentioned the existence of the aerosol layer. Is it impacting the transfer of radiation and the subsequent development of the boundary layer? How does it evolve? Can it be characterized (for instance with the aerosol optical depth)? It will be interesting to discuss the role of these observed aerosols on the boundary layer and the entrainment zone (see for instance Yu et al. J. Geophys. Res. 107, D124142 (2002) or Barbaro et al. J. Geophys. Res. 119, doi:10.1002/2013JD021237 (2014).

The height of the mentioned aerosol layer referred to the height of a temperature inversion which marks the top of the residual layer at night and at early morning. At this time we observed only low particle number concentration within the residual layer and much lower in the free troposphere. Figure 5 shows the global radiation observed on Mount Kleiner Feldberg. The global radiation increased after sunrise similar to the previous days but decreased substantially after clouds formation occurs around 9 to 10 UTC above the measurement site. We don't think that the small amount of particles have significantly

impact on the radiation budget in the morning and the growth of boundary layer. We agree that there are additional interesting areas (ex. impact of cloud shaddows) that require further research, but we think that this is beyond the scope of this study.

4) I have two major comments in the discussion.
The first one is related to the role of clouds. In the discussion the ventilation of atmospheric compounds from the PBL intro the free troposphere driven by the mass flux is not mentioned neither discussed. In my opinion, boundary layer height and the transport by mass flux is an important contribution to the budget of the atmospheric components in the sub-cloud layer. Mass flux influences boundary layer height according to (see Equation 4 at Ouwersloot et al., 2014, J. Geophysical Research 118, doi: 10.1002/2013D020431, 2013)):
(dh/dt) = we + ws + wm, [1] where (dh/dt) is the boundary layer growth, we the entrainment velocity, ws the subsidence motion and wm is the mass flux velocity. This mass flux leads to a reduction of the boundary layer growth and dominates also the vertical transport of atmospheric compounds (see Equation 3 at Ouwersloot et al, 2014). For instance, it leads to drying of the sub-cloud layer. The authors mentioned the descending air between the clouds resulting from the presence of roll vortices, but I believe it is necessary to include in the discussion how the mass flux influence the transport of ozone and CO2 in the studied case. In other words, it is necessary to show that the descending air between the clouds (1st paragraph at page 29188) is as important as the mass flux vertical mixing contribution. Note that once the air is introduced in the cloud layer, the stability of the environment diminish the capacity of mixing and therefore the downward transport of atmospheric components (see figure 10a at Vrezijbergh et al., Atmospheric Chemistry and Physics 9, 1289-1301, 2009)

We agree that a clear identification of the mass flux and mixing air masses would be the ideal case to identify individual contributions to the observed mixing signature in our data.
We think that the vertical upward mass flux is essential for the redistribution of the tracer signatures. Indeed air masses from the surface are lifted below the clouds and may keep their signature particularly under conditions of reduced mixing, which are evident in our data. We think we flew through such air masses in regions where the cloud or parts of the cloud already dissolved. As a result one would expect large variability of tracers since the mixing has not yet homogenized tracer gradients between the different air masses involved. This is indicated by the double peak structure with the CO2 profile during the mixing event, one peak in the subcloud-layer and one peak where the cloud dissolved (as also concluded by Vila et al 2005).
However, we have no additional in flight data which allow to identify the different flux contributions, but we think, that the observed tracer signature is the result from the combination of different mass fluxes and the subsequent mixing.

We included into the section 4.2:
The descending air in between the clouds can be affected by air, which has been uplifted by convective motions. The mass flux dominates mostly the vertical transport of atmospheric compounds from the PBL into the FT (Vila et al 2005, Ouwersloot et al 2013).

Connected to this, this section needs to be more quantitative in the description of clouds. At the last paragraph at page 29187 it is mentioned that the clouds are driven
by shallow convection (typical cloud covers 20%) whereas at the second paragraph at page 29190, they mentioned that there is a large cloud fraction. The authors needs to provide and discuss of the evolution of the cloud cover during the analysed day.

We added the evolution of the total cloud cover provided by Eumetsat to the supplement. North-west of the studied region one can recognize that high and mid level clouds are advected towards the measurement area. We extracted the total cloud cover over the measurement site from the COSMO-7 model. The total cloud cover increases from the morning to the afternoon up to 100 % in the late afternoon. Figure 4 gives an idea of the different cloud layers at different layers at 10 UTC. It is true that the cloud cover in the lower atmosphere is driven by the observed cloud streets while the total cloud cover increases during the day. We replaced "large cloud fraction" with "cumulus clouds" and the sentence on page 29190 reads now:

Since the measurements site is covered by cumulus clouds (see Fig. 4), it is obvious that particles larger than 100 nm are activated to form cloud droplets.

5) My second comment is related to the relation between ABL growth and entrainment (last paragraph section 4.2 at page 29188). As equation [1] indicates there are other processes that influence boundary layer growth. I disagree with the statement that subsidence (ws) limits entrainment. From Equation it can be seen that assuming no clouds (wm=0), (dh/dt) can become 0 (no growth ABL) in the case that the entrainment velocity is equal to the subsidence. I other words, entrainment is still a relevant process (since we>0) in spite there is not boundary layer growth. Similar to clouds, here large scale subsidence is mentioned, but it is not quantified. I believe this information is useful to complete the case description and it can be extracted from a meteorological model (COSMO, WRF or ECMWF).

We agree and rechecked charts from different models. The measurement site was not located within the center of the high pressure system (Fig. 4) and therefore the influence of large scale subsidence is weak. We agree with the reviewer that the subsidence might be insignificant for the boundary layer growth and entrainment in this study. We changed the section accordingly which reads now as follows:

Therefore, the growth of the PBL is an indication of entrainment from the FT into the PBL. On the other hand the increase of the temperature inversion (cause from large-scale subsidence) provides strengthening of the inversion layer and limited the further boundary layer growth, but entrainment still occurs (Ouwersloot et al, 2013).

References:

Ouwersloot, H. G., de Arellano, J. V.-G., H. van Stratum, B. J., Krol, M. C., & Lelieveld, J. (2013). Quantifying the transport of subcloud layer reactants by shallow cumulus clouds over the Amazon. Journal of Geophysical Research: Atmospheres, 118(23), 13,041–13,059. http://doi.org/10.1002/2013JD020431

Vilà-Guerau de Arellano, J., Kim, S.-W., Barth, M. C., & Patton, E. G. (2005). Transport and chemical transformations influenced by shallow cumulus over land. Atmospheric Chemistry and Physics, 5(12), 3219–3231. http://doi.org/10.5194/acp-5-3219-2005

We would like to thank both anonymous referees for their valuable comments on the manuscript which led to a significant improvement of the manuscript. According to the reviewers suggestions we included an additional Figure (now Figure 6). For the specific replys below we refer to the figure numbering of the original version. Referee #2 comments are given in bold, the answers in standard font. Changes to the text are in italics.

Comments

The impact of the paper could be enhanced by drawing more connections with current research. The introduction is excellent and thoroughly describes many of the foundations for this work. But it isn't completely clear to me how this research that carefully examines a single event can be used for future studies. Will it be necessary to have the complete suite of measurements and analyses presented here to interrogate mixing? Do clouds regularly drive this sort of mixing, and can these results be expected for other locations? Is CO2 a reliable tracer for mixing between the free troposphere and PBL? Can anything be said more generally about when and where this sort of mixing can be expected?

The questions are repeated below including specific comments and are answered there.

If it is possible to make more general statements about the case study presented here, then the results may be especially helpful for understanding ozone entrainment and mixing in the US. In the western US, vertical transport is particularly important for understanding compliance with air quality regulations, since ozone standards are tightening and some regions are strongly influenced by downward ozone transport from the FT. Referencing a few of the recent papers that discuss baseline ozone in the US and the contribution from downward mixing (e.g. Jaffe, ES&T, 2011; Cooper et al., Science, 2015; Lin et al., JGR, 2012) will help connect this work to a large and active research area.

We agree that the linkage to the studies in the US is relevant and included the following lines at P29174, L12:
Cooper et al (2015) highlighted that surface air quality regulations in the US strongly depend on accurate knowledge of baseline ozone, which is defined as ozone transported downwind from anthropogenic and natural sources, while forecast of baseline ozone needs large knowledge of all different transport processes. This includes intercontinental transport from Asia, which is often associated with episodes of enhanced ozone concentrations over large parts of the western US that is located at relatively high altitudes (Lin et al ,2012). Moreover, downward transport of ozone rich air from the FT can enhance ozone mixing ratio in the PBL (Beck et al., 1997, McKendry et al, 2000, Jaffe, 2011).

Many papers use CO rather than CO2 as a tracer for tropospheric air. Why is this the first use of CO2 and O3 to examine mixing (pg 29175, line 6), as both molecules are regularly measured? Justifying the use of CO2, which can be influenced by the biosphere as well as anthropogenic emissions, would be helpful. CO2 has been used as a tracer for pollution in winter, but in summer CO2's utility as a tracer is diminished because uptake and respiration introduces considerable variability. Noting the limitations for using CO2 to diagnose mixing would be helpful. CO2 variability is used here as an indicator of mixing. Quantifying this variability will help to connect these results with other studies. The mixing lines are a consequence of CO2 and O3 differences between the free troposphere and PBL, and comparing the variability to this difference may also provide a metric that could be used to quantify mixing.

We agree that we need to extend the discussion on CO2 as tracer and its limitations. On the days studied in our case study, CO2 showed stable mixing ratios of about 386 ppm with a small variability of less than 0.5 ppm in the FT. Additionally, we demonstrate that the air mass in the PBL was not affected by long range transport within the FT, which is supported by backward tracjectories. Pataki et al 2005 showed that CO2 can be used as tracer when no major sink is available, which is the case for the FT. This gives confidence that CO2 can be used as a tracer to identify mixing events at this particular day. Importantly, the variability of CO2 near the surface is needed to identify potential mixing events, since this leads to the formation of a gradient at the inversion. During night time respiration and potential impact from anthropogenic emissions are expected to dominate the surface measurements for the period of our case study. During night we observe larger CO2 mixing ratios than during the day close to the surface in the PBL, which is also the case during the mixing event. The mixture consists of air masses of high CO2 from the early morning and of low CO2 from day.

We agree that CO or the combination of CO2 and CO would increase the potential to identify and interpret the mixing event, but CO measurements are not available for the specific time period.

We conclude that CO2 is not the perfect tracer to study mixing, especially when biogenic update cannot be excluded, but in our particular case with the given circumstances it can be used to identify mixing events. To the authors' knowledge, it is the first study which used CO2 as tracer for mixing at the PBL top along with the tracer-tracer correlation method.

The figures are clear, but some of the legends are confusing. The text describing figures 6 and 7 mentions panels a) and b), but those labels don't appear on the figures, or appear with the date so as to be confusing. For figures 6-8, the confusing date/time label should be removed, and the date should be mentioned in the caption (the time already is). The label in figure 8 that lists the time contradicts the caption. The legend for figure 5 should change "PBLH/RLH" to "aerosol layer height". I don't understand the CO2 scale at the top of figure 5. If the times are given in local solar time, then the "morning/noon/afternoon" labels could be removed to declutter the figure.

We improved the figures 5 – 9 as suggested. The CO2 scale in figure 5 helps to link this figure with Figure 6 and is valid for the CO2 profile at 8:00 UTC, for the two remaining profiles the origin of the x-axis was shifted to time of measurement (11:30 and 13:15 UTC).

Smaller comments
1) Verb tense switches inconsistently between past and present, which leads to some confusion. I recommend that all descriptions of the field measurements from 2011 be written in the past tense and all descriptions of the current analysis be written in the present tense. For example, section 2.2.2 "The pressure was obtained. . .". Section 3.2 "PBLH decreased. . ." and "air mass composition was probed. . ." Section 3.3 "residual layer was. . ." and "CO2 was again well mixed. . .". Section 4.2 "PBLH grew to . . ." Section 5 "PBL was convectively driven during that day. . ."
We improved the grammar of the manuscript. Please see the track changes.

2) Some of the terminology is unclear. The stable layer is mentioned in the 2nd sentence, but never again in the text, yet it shows up on the figures. The text should discuss more clearly when the term PBL is used, and when SL/RL are used. I don't understand the sentence pg 29174, line 17 that mentions the inversion layer. Which layer is this? And how does the barrier exhibit gradients?

We clarified the terminology throughout the manuscript and changed the respective sentence as follows:
However, the boundary layer inversion acts as a barrier for mixing and often exhibits strong trace gas gradients.

3) Please note time response for all the measurements 2.2.1, which will be important if variability is quantified.
We updated the time response for CO2 and O3 within the text.
The response time of the instruments (5%/95%) was 3 s (CO2) and 9 s (O3) and the final data correction accounted for different residence times in the inlet lines.

4) pg 29184, line 9: replace "not directly related to clouds" with a sentence that states the measurements were not obtained in clouds. Later, the importance of clouds was noted, and that the measurements are related to clouds.
Changed sentence to:
Since the aircraft was allowed only to operate in cloud-free conditions, the large humidity values were only observed within the PBL.

5) Why do the O3, CO2 and water mixing ratios change with altitude in the PBL, as shown in Fig 7? Is the potential temperature constant? Is the PBL well-mixed when there is a strong vertical gradient in mixing ratios?

We included an additional figure (now Figure 6, see response to reviewer #1). The potential temperature is constant within the PBL, which is an indication for neutral stratification. The variability of ozone, CO2 and water vapor is affected by different sources, which we cannot separate but may be related to upward mixing from the dissipating night-time stable layer. At this time in the morning the trace gases are not completely mixed. Later that day, the profiles of CO2 and O3 become more constant with altitude (see Figure 5, after 13 UTC). We think our study is related exactly to this transition from a state of incomplete mixing (with large tracer variability) to the well mixed state during day time.

Pg 29174, line 29: replace aloft with above
Changed

Pg 29175, line 21-23: remove sentence, as the air mass influences are described better in the next paragraph
Removed

Pg 29177, line 5: use m asl instead of km to be consistent with the rest of the paper
Changed

Pg 29177, line 3: describe the profiles more specifically: spirals, and give the radius of the spirals.
We modified the sentence:
The descending flight legs were flown in spirals with a diameter of about 10 to 15 km.

Pg 29178, line 24: replace an with a
Changed

Pg 29179, line 3: replace "in 10 min average" with "as 10 min averages"
Changed

Pg 29181, line 11: replace "High CO2 values" with "CO2"
Changed

Pg 29184, line 13-14: Remove "after discussing" and replace "we use these information" with "are used"
Changed

Pg 29185, line 5: replace sentence beginning with "In this altitude. . .." With "The EZ was sampled at this location and time".
Changed to :
The EZ was situated at this location and time.

Pg 29187, line 3: replace "has grown" with "grew".
Changed

Pg 29190, line 1: difference rather than differences
Changed

Pg 29192, line 4: ". . .lead to variability that can be characterized by mixing lines"
Changed
Fig 1 – include Mt Kleiner Feldberg on map
Included

Fig 5 caption: replace rain bow with Rainbow
Changed

Fig 7 caption: replace "related due to the mixed air masses.." with "influenced by mixing air masses from the PBL. . ."
Changed

Referenzes

Cooper, O. R., Langford, A. O., Parrish, D. D., & Fahey, D. W. (2015). Challenges of a lowered U.S. ozone standard. Science, 348(6239), 1096–1097. http://doi.org/10.1126/science.aaa5748

Jaffe, D. (2011). Relationship between surface and free tropospheric ozone in the Western U.S. Environmental Science & Technology, 45(2), 432–8. http://doi.org/10.1021/es1028102

Lin, M., Fiore, A. M., Horowitz, L. W., Cooper, O. R., Naik, V., Holloway, J., Wyman, B. (2012). Transport of Asian ozone pollution into surface air over the western United States in spring. Journal of Geophysical Research: Atmospheres, 117(4), 1–20. http://doi.org/10.1029/2011JD016961

Pataki, D. E., B. J. Tyler, R. E. Peterson, A. P. Nair, W. J. Steenburgh, and E. R. Pardyjak (2005), Can carbon dioxide be used as a tracer of urban atmospheric transport?, J. Geophys. Res., 110, D15102, doi:10.1029/2004JD005723.

Airborne observation of mixing across the entrainment zone during PARADE 2011

F. Berkes[1,2,a]**, P. Hoor**[1]**, H. Bozem**[1]**, D. Kunkel**[1]**, M. Sprenger**[3]**, and S. Henne**[4]

[1]Institute for Atmospheric Physics, Johannes Gutenberg University Mainz, Mainz, Germany
[2]Department of Atmospheric Chemistry, Max Planck Institute for Chemistry, Mainz, Germany
[3]Institute for Atmospheric and Climate Science, ETH Zurich, Zürich, Switzerland
[4]Empa Swiss Federal Laboratories for Materials Science and Technology, Dübendorf, Switzerland
[a]now at: Institute of Energy and Climate Research-8: Troposphere,
Forschungszentrum Jülich GmbH, Jülich, Germany

Correspondence to: F. Berkes (f.berkes@fz-juelich.de)

Abstract

This study presents the analysis of the structure and air mass characteristics of the lower atmosphere during the field campaign PARADE (PArticles and RAdicals: Diel observations of the impact of urban and biogenic Emissions) on Mount Kleiner Feldberg in southwestern Germany during late summer 2011. We analysed measurements of meteorological variables (temperature, moisture, pressure, wind speed and direction) from radio soundings and of chemical tracers (carbon dioxide, ozone) from aircraft measurements. We focus on the thermodynamic and dynamic properties, that control the chemical distribution of atmospheric constituents in the boundary layer. We show that the evolution of tracer profiles of CO_2 and O_3 indicate mixing across the inversion layer (or entrainment zone). This finding is supported by the analysis of tracer–tracer correlations which are indicative for mixing and the relation of tracer profiles in relation to the evolution of the boundary layer height deduced from radio soundings. The study shows the relevance of entrainment processes for the lower troposphere in general and specifically that the tracer–tracer correlation method can be used to identify mixing and irreversible exchange processes across the inversion layer.

1 Introduction

The evolution of the planetary boundary layer (PBL) from stably stratified in the morning to well mixed in the afternoon is a multifaceted process and potentially leads to enhanced mixing between the PBL and the free troposphere (FT) (Stull, 1988). At sunset, a stable boundary layer (SL) with low turbulence intensity grows near the surface (Mahrt, 2014). Between this layer and the FT, a neutrally stratified layer remains resulting from the decay of turbulence of the convective PBL during daytime. This layer, called the residual layer (RL), maintains the chemical composition of the original convective PBL (Stull, 1988). The turbulent-convective PBL and the overlaying FT are separated by the capping inversion, which often acts as a transport barrier. This barrier, which is indicated by changes of

2

the vertical gradients of temperature, humidity, aerosol content and chemical constituents, can be overcome by frontal activity (Sinclair et al., 2010). Frontal systems ahead of the respective cold and warm sectors of a cyclonic depression lead to vertical exchange between the PBL and the FT and potentially mix both air masses (Donnell et al., 2001). This is also the case for shallow and deep convection (e. g. Flaty et al., 1995; Hauf et al., 1995). The so called entrainment zone (EZ) is a layer of intermittent turbulence at the top of the PBL where air masses from the FT are entrained into the capping inversion and thus can interact with convective thermals from the PBL (e. g. Angevine, 2007; Bange et al., 2007). Based on LIDAR (Träumner et al., 2011), wind profiler (Cohn and Angevine, 2000) and ceilometer measurements (Eresmaa et al., 2006), the extent of the EZ was estimated to 20–40 % of the PBL depth (Martin et al., 2014).

Airborne flux measurements of heat and moisture were used to determine the impact of entrainment on their budgets (e. g. Driedonks and Tennekes, 1984; Canut et al., 2010), and to understand the influence of entrainment on the development of boundary layer clouds (Stevens et al., 2003) and the decay of stratocumulus clouds (e. g. Lilly, 1968). Malinowski et al. (2013) showed that turbulent mixing between the cloud top and the FT depends on the thermodynamic properties (static stability) and wind shear (dynamic instability). Moreover, radiative effects can change the entrainment flux at the cloud tops and lead to exchange and mixing as well between the FT and PBL (Moeng et al., 1999). Modelling studies revealed that changes of the (static) stability, low-level wind shear, and turbulent motions affect not only the growth of the boundary layer but also the entrainment at the PBL top (e.g. Driedonks and Tennekes, 1984; Sullivan et al., 1998; Cohen, 2000). Lock et al. (2000) showed that mixing and entrainment at the top of the PBL depend on the surface buoyancy flux, the inversion strength and on the influence of wind shear (Conzemius and Fedorovich, 2006).

In recent years substantial efforts have been made to understand the driving physical processes of temperature and humidity transport during the growth or decay of the PBL as summarized by Lothon et al. (2014). It is still difficult to quantify the role of the EZ for the mixing of trace gases, because of its high spatial, vertical and temporal

variability (Martin et al., 2014). Vila-Guerau de Arellano (2004) was able to show that the downward transport of CO_2 from the FT into the PBL can enhance or reduce CO_2 mixing ratios within the PBL which then can lead to a misinterpretation of possible CO_2 sources. Vertical gradients of ozone exist as well between the PBL and FT, and they are strongly affected by transport processes and chemical reactions. Measurements and modelling studies of O_3 revealed that convective transport of ozone precursors lead to chemical ozone formation in the FT and enhances the background concentrations (Hov and Flatoy, 1997; Henne et al., 2005). Cooper et al. (2015) highlighted that surface air quality regulations in the US strongly depend on accurate knowledge of baseline ozone, which is defined as ozone transported downwind from anthropogenic and natural sources, while forecast of baseline ozone needs large knowledge of all different transport processes. This includes intercontinental transport from Asia, which is often associated with episodes of enhanced ozone concentrations over large parts of the western US that is located at relatively high altitudes (Lin et al., 2012). Moreover, downward transport of ozone rich air from the FT can enhance ~~the~~ ozone mixing ratio in the PBL ~~, too~~ ~~(Beck et al., 1997; McKendry and Lundgren, 2000)~~(Beck et al., 1997; McKendry and Lundgren, 2

Neuman et al. (2012) used tracer–tracer (CO-O_3) correlations to identify the in-mixing of ozone from the FT into the PBL. This approach is commonly used to identify stratosphere–troposphere exchange (e.g., Fischer et al., 2000; Hoor, 2002). Generally the approach makes the assumption of two well-mixed reservoirs, which give rise to linear tracer–tracer relationships in the case of mixing. However, the ~~inversion~~ boundary layer acts as a barrier for mixing and often exhibits strong trace gas gradients. Therefore the distribution of data points in tracer–tracer scatter plots subdivide into distinct groups depending on the mixing ratios of the respective well mixed reservoirs. Mixing between these air masses leads to linear connections between these groups (mixing lines).

Handisides (2001) presented ozone and peroxy radical observations from the local valley and from Mount Kleiner Feldberg and linked his findings to transport within different boundary layer structures in summertime. Moreover during winter, Wetter (1998) observed on the top of Mount Kleiner Feldberg CO plumes transported out of the stable boundary layer be-

low the summit. In both studies the PBL structure was not investigated in detail. However, this is necessary to understand and interpret the temporal evolution of the spatial distribution of atmospheric trace species measured within and ~~aloft~~ above the PBL, especially over complex terrain where handover processes between the PBL and the FT are additionally triggered by thermally induced flow systems (Kossmann et al., 1999; Henne et al., 2004).

In this study, we will use CO_2 and O_3 to study mixing across the EZ with the tracer–tracer correlation method. Both trace species have been measured by aircraft during the field campaign PARADE at Mount Kleiner Feldberg in late summer 2011, and are used for the first time together to identify mixing and transport within this atmospheric region. Additionally we discuss possible processes which lead to mixing across the entrainment zone. In this context we focus on the boundary layer development and the weather conditions. We will first present the synoptic condition during the day of measurements and put it into perspective with the entire situation of the measurement campaign. We focus on the diurnal evolution of the boundary layer which we determined with balloon and ceilometer measurements. We then present the results of the aircraft trace species measurements. Finally, we discuss possible processes which may be responsible for the measured distribution of CO_2 and O_3 and its influence from local mixing and long-range transport.

2 Measurement and methods

2.1 PARADE 2011

The PARADE (PArticles and RAdicals: Diel observations of the impact of urban and biogenic Emissions) field campaign took place in August and September 2011 located at the Taunus Observatory at the summit of Mount Kleiner Feldberg (825 m a.s.l.), about 20 km northwest of Frankfurt am Main in southwestern Germany. ~~The area around Mount Kleiner Feldberg is characterized by either pristine or anthropogenically polluted air conditions depending on the prevailing wind direction. The~~ The goal of PARADE was to study the impact of summertime biogenic and urban emissions in a semi-remote environment. A comprehensive set

of measurements of several reactive species and meteorological variables were conducted during PARADE, also including in situ measurement of ozone, and carbon dioxide (Phillips et al., 2012; Bonn et al., 2014; Li et al., 2015).

Mount Kleiner Feldberg is mostly covered with coniferous forest, except on the top where the observations took place during PARADE. Meteorological measurements for temperature, wind, humidity, global radiation are performed by a permanently operating observatory of the German Weather Service (DWD) and of the State of Hessen environmental agency (HLUG) (Crowley et al., 2010). The station is known for its quite remote character under prevailing northwesterly winds (Klein et al., 2010). However, this rural region is affected by pollution from the Rhein-Main area (including the cities of Frankfurt/Main, Wiesbaden, and Mainz) when wind directions have a southerly component. The area north of Mount Mount Kleiner Feldberg (50–100 km) is less populated and without major industry. In the direct vicinity of Mount Kleiner Feldberg are few main roads, some small towns within 5 km, and two similar sized mountain peaks are located: Großer Feldberg (878 m) and Altkönig (798 m).

During this field campaign the synoptic conditions involved predominately south westerly winds, mainly related to troughs over the northeastern Atlantic and to high pressure systems over Central Europe. The south westerly winds advected enhanced levels of anthropogenic pollution to Kleiner Feldberg and were interrupted by northern to north easterly winds several times. In these cases the probed air masses showed rather low levels of anthropogenic pollution (Phillips et al., 2012). We will present additional details on the synoptic conditions below.

2.2 Measurements

2.2.1 Aircraft instrumentation

A P68D Partenavia turbo prop aircraft operated by Enviscope GmbH (www.enviscope.de, last access: 12 November 2014) was equipped with several instruments to perform measurements in and above the planetary boundary layer on three days (31 August,

6

2 September, 6 September 2011) during the campaign. The aircraft flew 5 research flights from Mainz to Mount Kleiner Feldberg. Ascending profiles were flown up and downstream of the surface station, while descending profiles were performed directly over Mount Kleiner Feldberg. The ascending flight legs were conducted in different regions and are not included in the averaged profiles of the following analysis. The descending flight legs were flown in spirals with a diameter of about 10 to 15 km. The maximum flight altitude was three km 3000 m asl and the flight time was approximately two to three hours. A typical flight track is shown in Fig. 1 and illustrates the sampling strategy. In total, 13 descent profiles were obtained at different locations and times for each variable.

CO_2 was measured with a modified commercial CO_2/H_2O analyser (LI-6262, LI-COR Inc.) with a total uncertainty of 0.55 ppmv (= one standard deviation σ) determined from regular in-flight calibrations and a time resolution of 1 Hz (Gurk et al., 2008). Ozone (O_3) was measured by UV absorption every 10 seconds with the commercial gas analyser O342M (Environnement S.A.) with a total uncertainty of 1.3 ppbv for a moist air mass with less than 10 g kg^{-1} specific humidity (Köllner, 2013). The response time of the instruments (5%/95%) was 3 s (CO_2) and 9 s (O_3) and the final data correction accounted for different residence times in the inlet lines. The ambient temperature and moisture were measured every second with a commercial HMP230 (Vaisala) with an accuracy of two to three percent for relative humidity and 0.5 °C for temperature. The ambient pressure (SETRA Model 270) was measured with accuracy of 0.55 hPa (pers. com., Enviscope GmbH). The particle number concentration was measured by the Optical Particle Counter (Grimm SKY-OPC 1.129) for a size range of 0.25–32 μm (32 channels) and a time resolution of 1 Hz . Additionally, particle number concentrations of particles with diameters between 10 nm and 5 μm were measured with a modified condensation particle counter (CPC-Modell 3007, TSI) every second. These measurements are reported for standard temperature (273.15 K) and pressure (1013.25 hPa) conditions (STP).

Three-second average measurements are analysed corresponding to a spatial resolution of about 150 m at an average aircraft velocity of 50 m s^{-1}. The aircraft descent took about 10 min, so that the 3 s data yielded a vertical resolution of three to four meters. For

further analysis of the vertical structure of the trace gases measurements between 1000 and 3000 m a.s.l. Kleiner Feldberg (approx. 150 m over the mountain summit), each vertical profile is linearly interpolated to a uniform vertical grid with 10 m resolution.

2.2.2 Surface-based and radiosonde measurements

Vertical profiles of temperature, relative humidity and position were obtained from 174 radiosondes (GRAW DFM-06, www.graw.de, last access: 12 November 2014). Four to ten radiosondes were launched each day, starting usually one hour before sunrise and ending one hour after sunset. The sampling rate of 1 Hz results in a vertical resolution of about 1–2 m. The data has been interpolated onto a equidistant vertical grid with 20 m resolution. The pressure is obtained from these observations. Wind speed and wind direction are calculated from temporal changes of the current position of the balloon relative to the surface station. The near surface temperature measurements were compared to the temperature measurement from the local observatory. The comparison revealed a high positive correlation with an $r^2 = 0.99$ and a mean absolute deviation of $|T_{RS} - T_{DWD}| = 0.56 \pm 0.50\,^\circ$C.

The Ceilometer CHM 15 k-x from Jenoptik (www.jenoptik.com, last access: 12.11.2014) is primarily designed to determine the cloudbase from 200 m to 15 km above ground. In the absence of clouds, the backscatter signal can also be used for detecting aerosol layers (Münkel et al., 2007). The laser emits a light pulse with a repetition rate of 5–7 kHz, a pulse time of 1 ns and a wavelength of $\lambda = 1064$ nm, with a vertical resolution of 15 m. Thus, every 30 s a vertical backscatter profile is obtained.

Surface based CO_2 measurements were performed with a commercial CO_2/H_2O analyser (LI-6262, LI-COR Inc.) with a total uncertainty of 2 ppmv determined from regular calibrations and a time resolution of 1 Hz. Additionally CO_2 was measured from the mobile laboratory (MoLa) (Drewnick et al., 2012) with ~~an~~ a commercial CO_2/H_2O analyser (LI-840, LI-COR Inc.) without regular calibrations and a separate inlet line. This data was provided as 10 min mean values and is only used here to illustrate the diurnal cycle of CO_2. Surface based ozone measurements were performed by various instruments with different techniques at different locations during this campaign. At Mount Kleiner Feldberg O_3 was

measured by UV absorption with a commercial O_3 analyser (Model 49, Thermo Environmental Instruments Inc.). The total uncertainty was 5 % (two σ) and the data were provided ~~in~~ as 10 ~~average~~ minute averages (Li et al., 2015). HLUG provides 30 minute averaged O_3 measurements using a commercial UV absorption instrument (API 400) (Crowley et al., 2010).

2.3 Determination of the planetary boundary layer height

The planetary boundary layer height (PBLH) was calculated from the radio soundings using the surface based bulk Richardson number Ri_B (Vogelezang and Holtslag, 1996; Seibert et al., 2000). The dimensionless bulk Richardson number Ri_B is defined as the ratio of the vertical stability and the vertical shear of the horizontal wind:

$$Ri_B = \frac{g}{\overline{\theta_v}} \frac{\Delta\theta_v \Delta z}{(\Delta u)^2 + (\Delta v)^2} \tag{1}$$

with g the gravitational acceleration, θ_v the virtual potential temperature, z the altitude, and u, v the horizontal wind components (Vogelezang and Holtslag, 1996). The differences Δ are obtained from the respective values at the surface and the layers above. Ri_B provides an appropriate measure to characterize the stratification of the atmosphere and to determine the PBLH. The thermal stratification is determined from the sign of the bulk Richardson number. The flow is statically stable if Ri_B is greater than zero, else statically unstable or neutral. Furthermore, if Ri_B is below a critical value, the flow will become dynamically unstable and marks the altitude between the turbulent boundary layer and the stable stratified free troposphere. We used a threshold value of $Ri_B = 0.38$ which distinguish between a turbulent (low values of Ri_B) and a stable (large values of Ri_B) boundary layer. The same value is also used in the mesoscale model that we will introduce later (Fay, 1998). For clarity, the threshold value has been varied between 0.2 and 0.5 following suggestions from Zilitinkevich and Baklanov (2002) and Zhang et al. (2014), however, with a negligible effect on the results.

9

The PBLH has further been determined with the ceilometer, following the approach from Schneider and Eixmann (2002), to observe the height of the aerosol layer more frequently than with the radio soundings. The method is based on iterative averaging of the backscatter profile. Once the mean value has decreased to half the maximum average value inside the PBL, this altitude is designated to be the PBLH. Additionally, the height of the residual layer can be determined with this method at night. For our analysis we excluded all backscatter profiles which were observed during cloudy conditions. The determined boundary layers of the remaining backscatter profiles are averaged on an hourly basis.

2.4 Lagrangian air mass analysis

For the surface observations 24 h backward trajectories were calculated using LAGRANTO (Wernli and Davies, 1997; Sprenger and Wernli, 2015) from the position of Mount Kleiner Feldberg at 200 m above surface level (approximately between the modeled and actual mountain height) at 12:00 UTC for each day of the campaign. For the aircraft observations 24 h backward trajectories were calculated every 10 s along the flight path for each individual flight using LAGRANTO. In both cases, the trajectories were driven by model wind fields from the COSMO-7 analysis (Doms, 2011; Doms et al., 2011), operated by Swiss National Weather Service (MeteoSwiss). The meteorological fields from COSMO-7 are available every hour, the horizontal resolution is about 7 km, and 61 vertical levels are used from the surface up to 20 hPa. The trajectories are calculated from the three dimensional, kinematic wind field, not taking into account additional parametrisations for convection or turbulence.

2.5 Synoptic conditions during PARADE 2011

The synoptic conditions were alternating mainly between two kinds of weather patterns. Prior to the start of the measurement period (15–18 August 2011) the situation was dominated by a low pressure system over northwestern Europe and a high pressure system over central Europe. On 19 August 2011 a cold front related to a low pressure system over the north sea passed over the measurement area. This was then followed by high pressure

conditions over central Europe (20–26 August 2011) with very warm and humid temperatures. This period was again succeeded by the passage of a low pressure system late in the day on 26 August 2011 which formed over the eastern Atlantic. This led to relatively low temperatures with $T_{max} < 14\,°C$ and continued until the end of August (31 August 2011). Similar conditions were found during the last days of the campaign, only interrupted by fair weather between the end of August and 4 September 2011.

This synoptic pattern is well reflected by the daily mean carbon dioxide (CO_2) mixing ratio observed at the surface for the entire campaign (Fig. 2). High CO_2 values showed larger values during high pressure conditions (gray area), while lower CO_2 values were observed during low pressure conditions (white area). Figure 3 shows that the near surface based LAGRANTO backward trajectories match well with these synoptic conditions. Clean air masses from the north-west to westerly direction over the North Atlantic are linked to low CO_2 mixing ratios, while enhanced CO_2 values are related to the potentially polluted continental regions in southerly wind directions or related to local fair weather conditions. Note that biogenic uptake of CO_2 through photosynthesis was of minor importance at the end of the European growing season and that the CO_2 flux was probably dominated by anthropogenic emissions (Rivier et al., 2010).

3 Results

3.1 Synoptic situation on 6 September 2011

In the following we focus on one particular day (6 September 2011) when two research flights were completed. The two flights were flown in a prefrontal high pressure zone with a cyclonic system in northern Europe and high pressure in the south (Fig. 4). The approaching frontal system was associated with high wind speeds over Central Europe, carrying air masses rapidly from the Atlantic Ocean to Central Europe. A first trough reached western Europe on 5 September 2011, and marked the beginning of a series of low pressure systems. The next low was already present over the British Isles. Its cold front was semi-

occluded with the prefrontal warm front. Part of this warm front was situated over north western France (Fig. 4). The strong westerly wind transported colder air masses from the Atlantic Ocean and fostered the evolution of small-scale convective cells.

3.2 Diurnal evolution of the boundary layer on 6 September 2011

In this section, we briefly discuss the diurnal evolution of the PBL on 6 September 2011. We show the temporal evolution of Ri_B over Mount Kleiner Feldberg (Fig. 5). The vertical profiles of Ri_B have been calculated solely from the radio soundings and were linearly interpolated between each profile in this figure. In the morning hours low values of Ri_B are confined to the lowest layers (so called stable boundary layer). The extent of these low values increases during the day up to 2000 m a.s.l.. This reflects the growth of the PBL. In the morning hours a second inversion layer was indicated by the radiosounding profiles at around 2000–2500 m a.s.l.. This inversion further coincides with an increased backscatter signal detected by the ceilometer. The backscatter signal is related to an aerosol layer as well as the bottom of shallow cumulus clouds and marks the altitude of the residual layer.

The stable and residual layers merged between 10:00 and 11:00 UTC, afterwards only a single layered structure (now refered to as ~~boundary layer~~planetary boundary layer (PBL)) is detectable. Figure 6 shows profiles of the virtual potential temperature, wind speed and wind direction from the radio soundings just before and after the flights during that day. The PBLH at 11:00 UTC is located at 1640 m a.s.l. with an inversion strength of about 3 K. The maximum PBLH of 1981 m a.s.l. occurred at 14:00 UTC, while the strengthening of the temperature inversion increased to about 10 K. ~~Later on the PBLH decreases~~ The wind direction within the PBL and FT was mostly constant during that day, whereas the wind speed increased within the FT and decreased within the PBL during the day. Later on, the PBLH decreased to about 500 m before the onset of precipitation at around 18:00 UTC ~~.~~ (Fig. 5).

The air mass composition ~~has been~~ was probed twice during this day. The first flight took place between 07:00 and 09:30 UTC, while the second flight was between 11:00 and 14:00 UTC. Thus, a composition change of the PBL was expected from flight one to flight

two, since the first flight took place before the two layers merged, while the second occurred after this event.

3.3 Vertical profiles of trace gases during the boundary layer growth

Figure 7 also shows CO_2 profiles for the morning (07:27 UTC), at noon (11:42 UTC) and afternoon (13:12 UTC). The profiles are color-coded with specific humidity along the flight leg. The PBLH (black dashed line) and residual layer height (gray line), derived from the gradient of the humidity profiles, correspond well to the derived boundary layer heights from the radiosonde measurements.

In the morning the vertical profiles of CO_2 clearly show the three-layer structure of the PBL (Fig. 7a). Within the stable layer we observed a large variability of CO_2 mixing ratios ranging between 380.0 ppmv and 394.3 ppmv below 1000 m altitude. Between 1000 and 2300 m a.s.l. the vertical profile of CO_2 in the residual layer ~~is~~ was almost constant with mean values $(\overline{CO_2})$ of 380.5 (± 0.16) ppmv, indicating that the residual layer ~~is~~ was well mixed. A strong CO_2 gradient at 2300 m a.s.l. reveals a sharp separation between the PBL and the FT which has a mean CO_2 of about 383.0 (± 0.58) ppmv. In the afternoon (13:12 UTC) CO_2 is again well mixed within the PBL with $\overline{CO_2} = 382.1$ (± 0.35) ppmv (see Fig. 5). A clear separation to the FT is evident again, with mean FT-CO_2 mixing ratios of 383.7 (± 0.38) ppmv.

The transition period between the measurements of these two profiles is characterized by a much more variable CO_2 profile, especially above the PBLH (Fig. 7b). CO_2 decreases within the PBL with a mean value of 382.9 (± 0.49) ppmv. Above 1500 m a.s.l. in the FT mean CO_2 mixing ratios show a double peaked structure with maximum values of almost 386 ppmv and minimum values of 382 ppmv. Thus, a large variability with altitude is evident. Above 2300 m a.s.l. CO_2 mixing ratios are more comparable again to mixing ratios observed in the morning and the afternoon with a mean value of 383.9 (± 0.61) ppmv.

The vertical profiles of O_3 show a similar temporal evolution development (Figs. 7 and 8). Largest O_3 values are found in the FT above the boundary layer throughout the day and exceed local PBL values by typically 10 ppbv. The only exception is the transition period at

13

11:42 UTC, when O_3 shows a large variability. As for CO_2 a double peak structure is evident, however, the maxima and minima are anti-correlated between CO_2 and O_3. Furthermore, O_3-minima and CO_2-maxima show large values of water vapor mixing ratio q_v. These values exceed the commonly measured humidity values (less than $2\,g\,kg^{-1}$) in the FT. Since the aircraft was allowed only to operate in cloud-free conditions, ~~these large values are not directly related to clouds~~the large humidity values were only observed within the PBL. We will now analyse in detail how this complex structure is related to the observed development of the boundary layer structure.

3.4 Mixing deduced from correlations

~~After discussing the~~ The vertical profiles of O_3 and CO_2 and their temporal evolution over the course of the day, ~~we use these information~~ are used to study a potential mixing event on 6 September 2011 above Mount Kleiner Feldberg. For this we now apply tracer–tracer correlations (e. g., Fischer et al., 2000; Hoor, 2002). Figure 9 shows the scatter plot between O_3 and CO_2 in the morning (07:27 UTC). Using the moisture information and mean values of CO_2 and O_3 it is possible to identify two separated air masses. The air mass in the residual and stable layers has low O_3 values and variable values of CO_2 and q_v. The air mass in the FT is rather characterized by larger values of O_3, low values of q_v and less variability in CO_2.

At 11:42 UTC the appearance of the scatter plot changes significantly (Fig. 10). The chemical characteristics of two different air masses still can be identified, of which one has the characteristics of a boundary layer air mass (larger values for q_v) and one of a FT air mass (lower values of q_v). However, the air mass in the FT shows now also a larger variability in CO_2 which we see as an indication of a PBL air mass that has entered the FT. Moreover, the O_3 mixing ratios in the PBL are also slightly increased which could be related to downward transport of an FT air mass.

Using now also the temporal and spatial information of the measured data points, a linear relationship between the FT and PBL air masses in the tracer–tracer scatter plot becomes evident (Fig. 10). This line is highlighted with the black boxes. These data points have been

measured consecutively in an altitude range between 1640–2200 m, which is just above the PBLH at 11:42 UTC (Fig. 5). ~~In this altitude the~~ The EZ was situated ~~during this~~ at this location and time. Thus we regard these data points as the result of mixing, and the observed linear tracer–tracer relationship as mixing line, since it relates to the evolution of the boundary layer structure during this day. The specific humidity of this mixing line shows a slightly larger variability than the variability of the FT background (Fig. 8). This further supports our hypothesis of measuring a rather fresh mixing event. Note further that during this time clouds were present in the observation area with the cloud tops at around 2400 m a.s.l., according to the on board observations and a post flight analysis of photos taken during the flight. However, the strong variations of ozone, moisture and CO_2 for the profile at 11:42 (Fig. 7) have been observed exclusively in between clouds.

In short, we identify local mixing between air masses from the PBL and the FT from the results of the tracer tracer correlation technique for the trace gases CO_2 and O_3. Additionally, this mixing is supported by a larger variability of the specific humidity within the mixing region. In the following subsections, we will discuss processes which might have contributed to this mixing event as well as if this mixing event was influenced by long-range transport.

4 Discussion

4.1 Impact of long-range transport?

The origin of the probed air masses is investigated with 24 h kinematic backward trajectories using LAGRANTO (see Sect. 2.4) for this one-day period. Figure 11 shows the zonal position of the backward trajectories along the flight path at release time (0 h), −12 and −24 h prior to the measurements. Additionally, the trajectories are color-coded with the ozone mixing ratio as measured onboard the aircraft. Ozone was chosen, as tracer in this figure, because of its strong vertical gradient. The ozone mixing ratio is averaged for the trajectory positions backward in time for each hour in bins of 0.5° longitude and 250 m altitude. The binning compromises all calculated trajectories and reflects the transport of air

for a time period 24 h before the observations for the second flight around noon. It is evident that the measurement region has been influenced by air masses from two different origins (Fig. 11). The trajectory analysis reveals that the air mass probed above 2000 m with large O_3 mixing ratios, has been transported rapidly from westerly directions towards the measurement site. Furthermore, only these trajectories reside within the FT with the high O_3 mixing ratios. The trajectories at lower levels indicate that the air mass at this altitude range with low O_3 mixing ratios, has been advected more slowly. Importantly, air masses initialized below 2000 m, thus mainly within the turbulent boundary layer, show a larger spread of the trajectories and tend to stay in the boundary layer corresponding to low ozone mixing ratios. A similar behaviour is evident from CO_2 (not shown) confirming a clear separation between free tropospheric and boundary layer transport.

We conclude that the entrainment zone separates ozone rich air masses, which were transported in the free troposphere with higher wind speed than from air masses, which resided in the boundary layer with lower wind speed, as indicated by the low ozone mixing ratios. The clear vertical separation of air masses between the FT and PBL is therefore reflected by the different chemical signature of the air masses and is an indication, that the two respective air masses were spatially separated. It is thus an indication that the air masses must have been mixed shortly before or at the measurement location.

4.2 Impact of the local boundary layer conditions and cloud development

We will now show, if local mixing between boundary layer air and the air in the free troposphere can explain the observed signatures of mixing. The PBLH reaches 1640 m a.s.l. with an inversion strength of 3 K at 11:00 UTC. The residual layer height in the morning, as identified from the ceilometer and secondary temperature inversions from the radio soundings, reaches 2100 m. From 11:42 to 13:12 UTC the PBLH has grown grew to 2000 m a.s.l. and reaches a temperature inversion strength of 8 to 10 K. On the one hand, the growth of the boundary layer since 11:42 UTC is an indication for further entrainment of the overlying air masses into the PBL, which lead to further mixing. On the other hand, the increase of

16

the inversion strength limits the entrainment from air above and also the upward transport to the FT and reduced mixing (Angevine, 2007).

As shown in Fig. 5 the boundary layer top during the measurements was affected by the occurrence of clouds. These clouds were aligned along straight lines (Fig. 12), which is also evident from satellite images (not shown). The presence of clouds can affect the strength of the inversion layer as well as of the mixing between PBL and FT. Stevens (2007) and Malinowski et al. (2011) showed that radiative cooling at the upper edge of the clouds promotes a downward mixing of air and thus influences the inversion strength and might also contribute to the observed mixing event by entrainment of dry air from the FT. This can be seen by the decrease of the mean specific humidity between 1640 and 2200 m a.s.l. from the morning ($\overline{q_v} = 2.8\,(\pm1.2)\,\mathrm{g\,kg^{-1}}$) to noon time ($\overline{q_v} = 2.1\,(\pm0.7)\,\mathrm{g\,kg^{-1}}$).

An important feature of these cloud structures is the formation of roll vortices, which are aligned along the axis of the cloud bands. The cloud bands can be regarded as an indicator of shallow convection within the boundary layer. Moist air is lifted from near the surface up to the top of the PBL where the clouds form and the air descends in-between the clouds. The indicated air motion contributes especially to a further mixing of the PBL air mass, but can also increase the mixing potential between the PBL and the FT. This can then result in the vertical profiles of CO_2 as observed between the morning and the afternoon on 6 September 2011 (see Fig. 6). Hägeli et al. (2000) observed similar relationships for temperature and for moisture profiles within the cloud free area between the cloud streets. It should be noted, that many experimental studies are restricted to cloud-free conditions as summarised by Kalthoff et al. (2013).

So we suggest that the mixing event is linked to the evolution of shallow convection and consecutive cloud formation at the top of the PBL. Therefore, we will discuss the three CO_2 profiles during this day (Fig. 7), which reflects the suspected dynamic processes from theoretical approaches (e.g. Etling and Brown, 1993; Lock et al., 2000; Stevens et al., 2003). The descending air in between the clouds can be affected by air, which has been uplifted by convective motions~~within the PBL~~. The mass flux dominates mostly the vertical transport of atmospheric compounds from the PBL into the

17

FT (Vila-Guerau de Arellano, 2005; Ouwersloot et al., 2013). As discussed before (Figs. 5 and 7), in the afternoon (11:42 UTC) the CO_2 profiles between 1600 to 2300 m show double peak CO_2-mixing ratios around $\sim$ 386 ppmv, which were only present near the surface in the morning. Since there are no significant sources or sinks of CO_2 in the FT, these enhanced values indicate that surface air has been lifted locally and remains at this altitude when the cloud dissolved (Vila-Guerau de Arellano, 2005). This is also the case for specific humidity and ozone at this height, which exhibit exactly the same air mass composition as previously observed at the surface.

In principle, high ozone values can also be the result of photochemical ozone production, but ozone production would not add more than a few ppb per day (Morris et al., 2010). Ouwersloot et al. (2013) showed that ozone can be influenced by UV radiation extinction by clouds and atmospheric compounds like NO and NO_2. However, the high ozone values are accompanied by low humidity, which indicates potential downward transport from higher altitudes. This is confirmed by 5 days backward trajectories (calculated with ECMWF analysis (0.5 °C horizontal resolution, 90 vertical layer, 3 h time resolution)), which show that these air masses reached a maximum height of about 6 km over the Atlantic ocean, without any surface contact (not shown). Finally, during the entire day the specific humidity in the free troposphere showed very low mean values of 1.4 to 2.0 g kg^{-1}. This indicates that the free troposphere was dominated by an air mass of similar chemical characteristics during the measurements on the 6 September 2011. Between 2200–2500 m a.s.l. the ozone rich air mass is also observed with higher humidity. The variations of O_3, CO_2 and q_v above 2000 m clearly indicate layers of different origin in the region between 1600 and 2300 m a.s.l. in the cloud interstitial regions between the roll clouds.

Therefore, the growth of the PBL is an indication of entrainment from the FT into the PBL. On the other hand the increase of the temperature inversion (cause from large-scale subsidence) provides strengthening of the inversion layer and limited the further boundary layer growth and thus the entrainment (Arya, 2001), but entrainment still occurs (Ouwersloot et al., 2013).

4.3 Impact of mixing on surface measurements

It has previously been shown that boundary layer air trapped within the stable layer can suddenly be mixed in the newly growing PBL as soon as the PBL becomes unstable (Stull, 1988). In addition, large scale synoptic situations can lift these air masses out of the PBL into the FT (Sinclair et al., 2010). Vice versa, polluted plumes from the FT can enter the PBL by downward mixing and potentially lead to an increase of the pollution levels near the surface in initially clean regions (McKendry and Lundgren, 2000; Neuman et al., 2012).

Figure 13 shows the ozone mixing ratios onboard the aircraft and the time series at the surface. The airborne measurements below 800 m a.s.l. agree well with the surface observations of about 30 ppb. The higher values around 07:30 UTC observed onboard the aircraft can be explained by the fact, that the measurements directly at the surface are affected by deposition and ozone loss processes within the stable nocturnal boundary layer, which was not accessible for the aircraft. As shown in Fig. 5, around 09:00 UTC at the end of the first flight the stable layer of the lowest level disappears and is then mixed with the newly growing boundary layer. At this time, between the two flights, there occurs an increase of O_3 of 6 ppbv per hour up to a maximum mixing ratio of 43 ppbv at noon. The increase of ozone can be attributed to photochemical ozone production and downward mixing from the free troposphere. McKendry and Lundgren (2000) showed that an increase of the ozone mixing ratio larger than 5 ppbv h^{-1} has been related to downward transport from the FT and not to photochemical production alone. As mentioned earlier, clouds formed initially between 09:00–10:00 UTC. For that reason the global radiation decreased and hence the photochemical ozone production efficiency has been reduced (Fig. 5).

Figure 14 shows the CO_2 mixing ratio onboard the aircraft and near the surface. The airborne CO_2 measurements show low mixing ratios of 381 ppmv (8:00 UTC) compared to the high CO_2 surface measurements. This large ~~differences~~ difference is due to accumulated CO_2 in the stable boundary layer during night. This is consistent with slightly enhanced ozone measured onboard the aircraft for this period (see Fig. 13). The aircraft was always flying at least 100 m above the surface where the CO_2 values are already much lower com-

pared to the stable surface layer below. Note, that the CO_2 profile in Fig. 5 also indicates much higher CO_2 values at the lowest levels, which are in the same range as observed at the surface at Mount Kleiner Feldberg. Thus during night, CO_2 at the surface is dominated by plant respiration and anthropogenic CO_2 emissions. During day a potential effect from downward mixing at the surface is probably masked by some local uptake of CO_2 by vegetation.

The particle number concentration measurements show very low values of 1 to 2 particles ccm^{-1} within the FT. Within the PBL we observe larger particle number concentration from the CPC (210 particles ccm^{-1}) than from the OPC (40 particles ccm^{-1}). Since the measurements site is covered by ~~a large cloud fraction~~cumulus clouds (see fig. 4), it is obvious that particles larger than 100 nm were activated to form cloud droplets. These measurements could not be used to further support the mixing process. Furthermore, the backscatter signal from the ceilometer was mostly affected by the clouds (after 10:00 UTC) and therefore we observed only the cloud base height. The increase of O_3 near the surface is most likely the result of mixing of O_3 rich air masses from the FT. This downward transport process would match well with the time of occurrence of the mixing line.

5   Conclusions

Extensive surface based, balloon based and airborne measurements were collected as part of the measurement campaign PARADE on Mount Kleiner Feldberg (825 m) in summer 2011. We used this data to investigate the diurnal evolution of the boundary layer height over this complex terrain as well as the potential impact of local and long-range transport of trace gases. Our focus was on two research flights on 6 September 2011 where vertical tracer properties of CO_2 and O_3 indicated the occurrence of mixing across the entrainment zone. The planetary boundary layer height was determined using the Bulk-Richardson-number (Ri_B) from measurements taken from radio soundings. This approach can be used both under stable and unstable conditions using the same criteria. The boundary layer top grew from 860 m a.s.l. in the morning up to 2000 m a.s.l. in the afternoon. During this growth

it merged with the residual layer (2100 m a.s.l. at 06:00 UTC). Negative Ri_B values indicated that the PBL is convectively driven and turbulent during that day, and thus well mixed. Additionally, airborne measurements of various trace gases (CO_2 and O_3) and particle number concentrations were performed in cloud-free areas during that day.

The temporal evolution of the measured vertical trace gas profiles showed the evolution of the PBL as observed with the radio soundings. The merging of the stable boundary layer, residual layer and free troposphere with the convective driven boundary layer is involved with mixing of the trace gases from these different atmospheric layers, and lead to complex vertical profiles of the trace gases. The tracer–tracer correlations have been applied to identify this mixing event and the effect on the trace gas distribution change across the transport barrier at the boundary layer top. This mixing line is probably formed by vertical uplift of CO_2 rich and O_3 poor air masses from the morning stable boundary layer. The strong western wind transported cold air masses from the Atlantic Ocean and caused the development of cloud streets. The structure of the trace gas profiles resembles the vertical cloud structure. We found the mixed air masses in the cloud interstitial space. This is consistent with convective uplifting and mixing with FT air at the cloud top within the clouds and subsidence of outside the clouds. It is suggested that these conditions forced mixing between the FT and the PBL. It cannot be excluded that the mixing event was affected by long-range transport. The analysis of the local meteorological situation and the trace gas observations, however provide strong evidence, that the local boundary layer growth lead to mixing at the PBL top. This is supported by the specific humidity, which shows on the mixing line a slightly larger variability than the variability of the FT background humidity. The additional formation of shallow convective clouds at the PBL top (and roll convection) probably led to an efficient exchange between the boundary layer and the free troposphere.

We conclude, that rapid boundary layer growth and its interaction with convective clouds at the PBL top can efficiently mix both air masses and lead to ~~the occurrence of~~ variability that can be characterized by mixing lines. Moreover, the analysis of mixing lines provides a powerful tool to identify the occurrence and the effect of processes, which lead to a constituent exchange and mixing across the inversion layer.

21

References

Angevine, W. M.: Transitional, entraining, cloudy, and coastal boundary layers, Acta Geophys., 56, 2–20, doi:10.2478/s11600-007-0035-1, 2007.

Arya, S. P.: Introduction to Micrometeorology, vol. 79, 2nd edn., Academic Press, 2001.

Bange, J., Spieß, T., and van den Kroonenberg, A.: Characteristics of the early-morning shallow convective boundary layer from Helipod Flights during STINHO-2, Theor. Appl. Climatol., 90, 113–126, doi:10.1007/s00704-006-0272-2, 2007.

Beck, J. P., Asimakopoulos, N., Bazhanov, V., Bock, H. J., Chronopoulos, G., Muer, D. D., Ebel, A., Flatøy, F., Hass, H., van Haver, P., Hov, O., Jakobs, H. J., Kirchner, E. J. J., Kunz, H., Memmesheimer, M., van Pul, W. A. J., Speth, P., Trickl, T., and Varotsos, C.: Exchange of Ozone Between the Atmospheric Boundary Layer and the Free Troposphere, Springer-Verlag, doi:10.1007/978-3-642-58729-0_5, 1997.

Bonn, B., Bourtsoukidis, E., Sun, T. S., Bingemer, H., Rondo, L., Javed, U., Li, J., Axinte, R., Li, X., Brauers, T., Sonderfeld, H., Koppmann, R., Sogachev, A., Jacobi, S., and Spracklen, D. V.: The

link between atmospheric radicals and newly formed particles at a spruce forest site in Germany, Atmos. Chem. Phys., 14, 10823–10843, doi:10.5194/acp-14-10823-2014, 2014.

Canut, G., Lothon, M., Saïd, F., and Lohou, F.: Observation of entrainment at the interface between monsoon flow and the Saharan Air Layer, Q. J. Roy. Meteor. Soc., 136, 34–46, doi:10.1002/qj.471, 2010.

Cohen, C.: A Quantitative investigation of entrainment and detrainment in numerically simulated cumulonimbus clouds, J. Atmos. Sci., 57, 1657–1674, doi:10.1175/1520-0469(2000)057<1657:AQIOEA>2.0.CO;2, 2000.

Cohn, S. A. and Angevine, W. M.: Boundary layer height and entrainment zone thickness measured by lidars and wind-profiling radars, J. Appl. Meteorol., 39, 1233–1247, doi:10.1175/1520-0450(2000)039<1233:BLHAEZ>2.0.CO;2, 2000.

Conzemius, R. J. and Fedorovich, E.: Dynamics of sheared convective boundary layer entrainment. Part I: Methodological background and large-eddy simulations, J. Atmos. Sci., 63, 1151–1178, doi:10.1175/JAS3691.1, 2006.

Cooper, O. R., Langford, A. O., Parrish, David D. and Fahey, David W.: Challenges of a lowered U.S. ozone standard, Science, 6239, 1096–1097, doi:10.1126/science.aaa5748, 2015.

Crowley, J. N., Schuster, G., Pouvesle, N., Parchatka, U., Fischer, H., Bonn, B., Bingemer, H., and Lelieveld, J.: Nocturnal nitrogen oxides at a rural mountain-site in south-western Germany, Atmos. Chem. Phys., 10, 2795–2812, doi:10.5194/acp-10-2795-2010, 2010.

Doms, D.: A description of the nonhydrostatic regional COSMO-model, Part I: Dynamics and numerics, Tech. rep., Deutscher Wetterdienst, 2011.

Doms, D., Förstner, J., Heise, E., Herzog, H., Mironov, D., Raschendorfer, M., Reinhardt, T., Ritter, B., Schrodin, R., Schulz, J., and Vogel, G.: A description of the nonhydrostatic regional COSMO-model, Part II: Physical parameterization, Tech. rep., Deutscher Wetterdienst, 2011.

Donnell, E. A., Fish, D. J., Dicks, E. M., and Thorpe, A. J.: Mechanisms for pollutant transport between the boundary layer and the free troposphere, J. Geophys. Res., 106, 7847, doi:10.1029/2000JD900730, 2001.

Drewnick, F., Böttger, T., von der Weiden-Reinmüller, S.-L., Zorn, S. R., Klimach, T., Schneider, J., and Borrmann, S.: Design of a mobile aerosol research laboratory and data processing tools for effective stationary and mobile field measurements, Atmos. Meas. Tech., 5, 1443–1457, doi:10.5194/amt-5-1443-2012, 2012.

Driedonks, A. and Tennekes, H.: Entrainment effects in the well-mixed atmospheric boundary layer, Bound.-Lay. Meteorol., 30, 75–105, doi:10.1007/978-94-009-6514-0_4, 1984.

Eresmaa, N., Karppinen, A., Joffre, S. M., Räsänen, J., and Talvitie, H.: Mixing height determination by ceilometer, Atmos. Chem. Phys., 6, 1485–1493, doi:10.5194/acp-6-1485-2006, 2006.

Etling, D. and Brown, R. A.: Roll vortices in the planetary boundary layer: A review, Bound.-Lay. Meteorol., 65, 215–248, doi:10.1007/BF00705527, 1993.

Fay, B.: Evaluation and intercomparison of mixing heights based on the new prognostic turbulence scheme of the pre-operational limited area model at the german weather service, in: Harmo5 Conf., Rhodes, 1998.

Fischer, H., Wienhold, F. G., Hoor, P., Bujok, O., Schiller, C., Siegmund, P., Ambaum, M., Scheeren, H. A., and Lelieveld, J.: Tracer correlations in the northern high latitude lowermost stratosphere: Influence of cross-tropopause mass exchange, Geophys. Res. Lett., 27, 97–100, doi:10.1029/1999GL010879, 2000.

Flaty, F., Hov, O., and Smit, H.: Three-dimensional model studies of exchange processes of ozone in the troposphere over Europe, J. Geophys. Res., 100, 11465–11481, doi:10.1029/95JD00845, 1995.

Gurk, C., Fischer, H., Hoor, P., Lawrence, M.G., Lelieveld, J., and Wernli, H.: Airborne in-situ measurements of vertical, seasonal and latitudinal distributions of carbon dioxide over Europe, Atmos. Chem. Phys. Discuss., 8, 7315–7337, doi:10.5194/acpd-8-7315-2008, 2008.

Hägeli, P., Steyn, D. G., and Strawbridge, K. B.: Spatial and temporal variability of mixed-layer depth and entrainment zone thickness, Bound.-Lay. Meteorol., 96, 47–71, doi:10.1023/A:1002790424133, 2000.

Handisides, G. M.: The influence of peroxy radicals on ozone production, Dissertation, 2001.

Hauf, T., Schulte, P., Alheit, R., and Schlager, H.: Rapid vertical trace gas transport by an isolated midlatitude thunderstorm, J. Geophys. Res., 100, 22957–22970, doi:10.1029/95JD02324, 1995.

Henne, S., Furger, M., Nyeki, S., Steinbacher, M., Neininger, B., de Wekker, S. F. J., Dommen, J., Spichtinger, N., Stohl, A., and Prévôt, A. S. H.: Quantification of topographic venting of boundary layer air to the free troposphere, Atmos. Chem. Phys., 4, 497–509, doi:10.5194/acp-4-497-2004, 2004.

Henne, S., Dommen, J., Neininger, B., Reimann, S., Staehelin, J., and Prevot, A. S. H.: Influence of mountain venting in the Alps on the ozone chemistry of the lower free troposphere and the European pollution export, J. Geophys. Res.-Atmos., 110, D22307, doi:10.1029/2005JD005936, 2005.

24

Hoor, P.: Seasonal variations of a mixing layer in the lowermost stratosphere as identified by the CO-O 3 correlation from in situ measurements, J. Geophys. Res., 107, 4044, doi:10.1029/2000JD000289, 2002.

Hov, O. and Flatoy, F.: Convective redistribution of ozone and oxides of nitrogen in the troposphere over Europe in summer and fall, J. Atmos. Chem., 28, 319–337, doi:10.1023/A:1005780730600, 1997.

Jaffe, Dan: Relationship between surface and free tropospheric ozone in the Western U.S., Environmental science & technology, 45, 432–438, doi:10.1021/es1028102, 2011.

Kalthoff, N., Träumner, K., Adler, B., Späth, S., Behrendt, A., Wieser, A., Handwerker, J., Madonna, F., and Wulfmeyer, V.: Dry and moist convection in the boundary layer over the Black Forest – a combined analysis of in situ and remote sensing data, Meteorol. Z., 22, 445–461, doi:10.1127/0941-2948/2013/0417, 2013.

Klein, H., Nickovic, S., Haunold, W., Bundke, U., Nillius, B., Ebert, M., Weinbruch, S., Schuetz, L., Levin, Z., Barrie, L. A., and Bingemer, H.: Saharan dust and ice nuclei over Central Europe, Atmos. Chem. Phys., 10, 10211–10221, doi:10.5194/acp-10-10211-2010, 2010.

Köllner, F.: Charakterisierung und Einsatz eines flugzeuggetragenen Ozonmessgerätes in der Grenzschicht, Thesis, Johannes-Gutenberg Universität, Mainz, 2013.

Kossmann, M., Corsmeier, U., De Wekker, S. F., Fiedler, F., Vögtlin, R., Kalthoff, N., Güsten, H., and Neininger, B.: Observations of handover processes between the atmospheric boundary layer and the free troposphere over mountaineous terrain, Contributions to Atmospheric Physics, 72, 329–350, 1999.

Li, J., Reiffs, A., Parchatka, U., and Fischer, H.: In situ measurements of atmospheric CO and its correlation with NO_x and O_3 at a rural mountain site, Metrol. Meas Syst., 22, 25–38, 2015.

Lilly, D. K.: Models cloud-topped mixed layers under a strong inversion, Tech. Rep. July 1967, 1968.

Lin, Meiyun and Fiore, Arlene M. and Horowitz, Larry W. and Cooper, Owen R. and Naik, Vaishali and Holloway, John and Johnson, Bryan J. and Middlebrook, Ann M. and Oltmans, Samuel J. and Pollack, Ilana B. and Ryerson, Tomas B. and Warner, Juying X. and Wiedinmyer, Christine and Wilson, John and Wyman, Bruce: Transport of Asian ozone pollution into surface air over the western United States in spring, J. Geophys. Res.-Atmos., 117, 1–20, doi:10.1029/2011JD016961, 2012.

Lock, A. P., Brown, A. R., Bush, M. R., Martin, G. M., Smith, R. N. B., Ock, A. P. L., Rown, A. R. B., Ush, M. R. B., and Artin, G. M. M.: A new boundary layer mixing scheme. Part I: Scheme de-

25

scription and single-column model tests, Mon. Weather Rev., 128, 3187–3199, doi:10.1175/1520-0493(2000)128<3187:ANBLMS>2.0.CO;2, 2000.

Lothon, M., Lohou, F., Pino, D., Couvreux, F., Pardyjak, E. R., Reuder, J., Vilà-Guerau de Arellano, J., Durand, P., Hartogensis, O., Legain, D., Augustin, P., Gioli, B., Faloona, I., Yagüe, C., Alexander, D. C., Angevine, W. M., Bargain, E., Barrié, J., Bazile, E., Bezombes, Y., Blay-Carreras, E., van de Boer, A., Boichard, J. L., Bourdon, A., Butet, A., Campistron, B., de Coster, O., Cuxart, J., Dabas, A., Darbieu, C., Deboudt, K., Delbarre, H., Derrien, S., Flament, P., Fourmentin, M., Garai, A., Gibert, F., Graf, A., Groebner, J., Guichard, F., Jimenez Cortes, M. A., Jonassen, M., van den Kroonenberg, A., Lenschow, D. H., Magliulo, V., Martin, S., Martinez, D., Mastrorillo, L., Moene, A. F., Molinos, F., Moulin, E., Pietersen, H. P., Piguet, B., Pique, E., Román-Cascón, C., Rufin-Soler, C., Saïd, F., Sastre-Marugán, M., Seity, Y., Steeneveld, G. J., Toscano, P., Traullé, O., Tzanos, D., Wacker, S., Wildmann, N., and Zaldei, A.: The BLLAST field experiment: Boundary-Layer Late Afternoon and Sunset Turbulence, Atmos. Chem. Phys. Discuss., 14, 10789–10852, doi:10.5194/acpd-14-10789-2014, 2014.

Mahrt, L.: Stably stratified atmospheric boundary layers, Annu. Rev. Fluid Mech., 46, 23–45, doi:10.1146/annurev-fluid-010313-141354, 2014.

Malinowski, S. P., Haman, K. E., Kopec, M. K., Kumala, W., and Gerber, H.: Small-scale turbulent mixing at stratocumulus top observed by means of high resolution airborne temperature and LWC measurements, J. Phys. Conf. Ser., 318, 072013, doi:10.1088/1742-6596/318/7/072013, 2011.

Malinowski, S. P., Gerber, H., Jen-La Plante, I., Kopec, M. K., Kumala, W., Nurowska, K., Chuang, P. Y., Khelif, D., and Haman, K. E.: Physics of Stratocumulus Top (POST): turbulent mixing across capping inversion, Atmos. Chem. Phys., 13, 12171–12186, doi:10.5194/acp-13-12171-2013, 2013.

Martin, S., Beyrich, F., and Bange, J.: Observing entrainment processes using a small unmanned aerial vehicle: a feasibility study, Bound.-Lay. Meteorol., 150, 449–467, doi:10.1007/s10546-013-9880-4, 2014.

McKendry, I. and Lundgren, J.: Tropospheric layering of ozone in regions of urbanized complex and/or coastal terrain: a review, Prog. Phys. Geog., 24, 329–354, doi:10.1177/030913330002400302, 2000.

Moeng, C.-M., Sullivan, P. P., and Stevens, B.: Including radiative effects in an entrainment rate formula for buoyancy-driven PBLs, J. Atmos. Sci., 56, 1031–1049, 1999.

Morris, G. A., Ford, B., Rappenglück, B., Thompson, A. M., Mefferd, A., Ngan, F., and Lefer, B.: An evaluation of the interaction of morning residual layer and afternoon mixed layer ozone in Houston

26

using ozonesonde data, Atmos. Environ., 44, 4024–4034, doi:10.1016/j.atmosenv.2009.06.057, 2010.

Münkel, C., Eresmaa, N., Räsänen, J., and Karppinen, A.: Retrieval of mixing height and dust concentration with lidar ceilometer, Bound.-Lay. Meteorol., 124, 117–128, doi:10.1007/s10546-006-9103-3, 2007.

Neuman, J. A., Trainer, M., Aikin, K. C., Angevine, W. M., Brioude, J., Brown, S. S., de Gouw, J. A., Dube, W. P., Flynn, J. H., Graus, M., Holloway, J. S., Lefer, B. L., Nedelec, P., Nowak, J. B., Parrish, D. D., Pollack, I. B., Roberts, J. M., Ryerson, T. B., Smit, H., Thouret, V., and Wagner, N. L.: Observations of ozone transport from the free troposphere to the Los Angeles basin, J. Geophys. Res.-Atmos., 117, D00V09, doi:10.1029/2011JD016919, 2012.

Ouwersloot, H. G. and de Arellano, J. Vilà-Guerau and H. van Stratum, B. J. and Krol, M. C. and Lelieveld, J.: Quantifying the transport of subcloud layer reactants by shallow cumulus clouds over the Amazon, J. Geophys. Res.-Atmos., 118, 13041–13059, doi:10.1002/2013JD020431, 2013.

Phillips, G. J., Tang, M. J., Thieser, J., Brickwedde, B., Schuster, G., Bohn, B., Lelieveld, J., and Crowley, J. N.: Significant concentrations of nitryl chloride observed in rural continental Europe associated with the influence of sea salt chloride and anthropogenic emissions, Geophys. Res. Lett., 39, L10811, doi:10.1029/2012GL051912, 2012.

Rivier, L., Peylin, P., Ciais, P., Gloor, M., Rödenbeck, C., Geels, C., Karstens, U., Bousquet, P., Brandt, J., and Heimann, M.: European CO_2 fluxes from atmospheric inversions using regional and global transport models, Climatic Change, 103, 93–115, doi:10.1007/s10584-010-9908-4, 2010.

Schneider, J. and Eixmann, R.: Three years of routine Raman lidar measurements of tropospheric aerosols: Backscattering, extinction, and residual layer height, Atmos. Chem. Phys., 2, 313–323, doi:10.5194/acp-2-313-2002, 2002.

Seibert, P., Beyrich, F., Gryning, S.-E., Joffre, S., and Rasmussen, A.: Review and intercomparison of operational methods for the determination of the mixing height, Atmos. Environ., 34, 1001–1027, doi:10.1016/S1352-2310(99)00349-0, 2000.

Sinclair, V. A., Gray, S. L., and Belcher, S. E.: Controls on boundary layer ventilation: Boundary layer processes and large-scale dynamics, J. Geophys. Res., 115, D11107, doi:10.1029/2009JD012169, 2010.

Sprenger, M. and Wernli, H.: The Lagrangian analysis tool LAGRANTO – version 2.0, Geosci. Model Dev. Discuss., 8, 1893–1943, doi:10.5194/gmdd-8-1893-2015, 2015.

Stevens, B.: On the growth of layers of nonprecipitating cumulus convection, J. Atmos. Sci., 64, 2916–2931, doi:10.1175/JAS3983.1, 2007.

Stevens, B., Lenschow, D. H., Vali, G., Gerber, H., Bandy, A., Blomquist, B., Brenguier, J.-L., Bretherton, C. S., Burnet, F., Campos, T., Chai, S., Faloona, I., Friesen, D., Haimov, S., Laursen, K., Lilly, D. K., Loehrer, S. M., Malinowski, S. P., Morley, B., Petters, M. D., Rogers, D. C., Russell, L., Savic-Jovcic, V., Snider, J. R., Straub, D., Szumowski, M. J., Takagi, H., Thornton, D. C., Tschudi, M., Twohy, C., Wetzel, M., and van Zanten, M. C.: Dynamics and chemistry of marine stratocumulus DYCOMS-II, B. Am. Meteorol. Soc., 84, 579–593, doi:10.1175/BAMS-84-5-579, 2003.

Stull, R. B.: An Introduction to Boundary Layer Meteorology, vol. 13, Springer, the Netherlands, Dordrecht, doi:10.1007/978-94-009-3027-8, 1988.

Sullivan, P. P., Moeng, C.-H., Stevens, B., Lenschow, D. H., and Mayor, S. D.: Structure of the entrainment zone capping the convective atmospheric boundary layer, J. Atmos. Sci., 55, 3042–3064, doi:10.1175/1520-0469(1998)055<3042:SOTEZC>2.0.CO;2, 1998.

Träumner, K., Kottmeier, C., Corsmeier, U., and Wieser, A.: Convective boundary-layer entrainment: short review and progress using doppler lidar, Bound.-Lay. Meteorol., 141, 369–391, doi:10.1007/s10546-011-9657-6, 2011.

Vila-Guerau de Arellano, J.: Entrainment process of carbon dioxide in the atmospheric boundary layer, J. Geophys. Res., 109, D18110, doi:10.1029/2004JD004725, 2004.

Vila-Guerau de Arellano, J., Kim, S.-W. and Barth, M. C. and Patton, E. G.: Transport and chemical transformations influenced by shallow cumulus over land, Atmos. Chem. Phys., 12, 3219–3231, doi:10.5194/acp-5-3219-2005, 2005.

Vogelezang, D. and Holtslag, A.: Evaluation and model impacts of alternative boundary-layer height formulations, Bound.-Lay. Meteorol., 81, 245–269, doi:10.1007/BF02430331, 1996.

Wernli, H. and Davies, H. C.: A lagrangian-based analysis of extratropical cyclones. I: The method and some applications, Q. J. Roy. Meteor. Soc., 123, 467–489, doi:10.1002/qj.49712353811, 1997.

Wetter, T.: Messungen des CO- und H_2-Mischungsverhältnisses im Winter 1996/97, Thesis, 1998.

Zhang, Y., Gao, Z., Li, D., Li, Y., Zhang, N., Zhao, X., and Chen, J.: On the computation of planetary boundary layer height using the bulk Richardson number method, Geosci. Model Dev. Discuss., 7, 4045–4079, doi:10.5194/gmdd-7-4045-2014, 2014.

Zilitinkevich, S. and Baklanov, A.: Calculation of the height of the stable boundary layer in practical applications, Bound.-Lay. Meteorol., 105, 389–409, doi:10.1023/A:1020376832738, 2002.
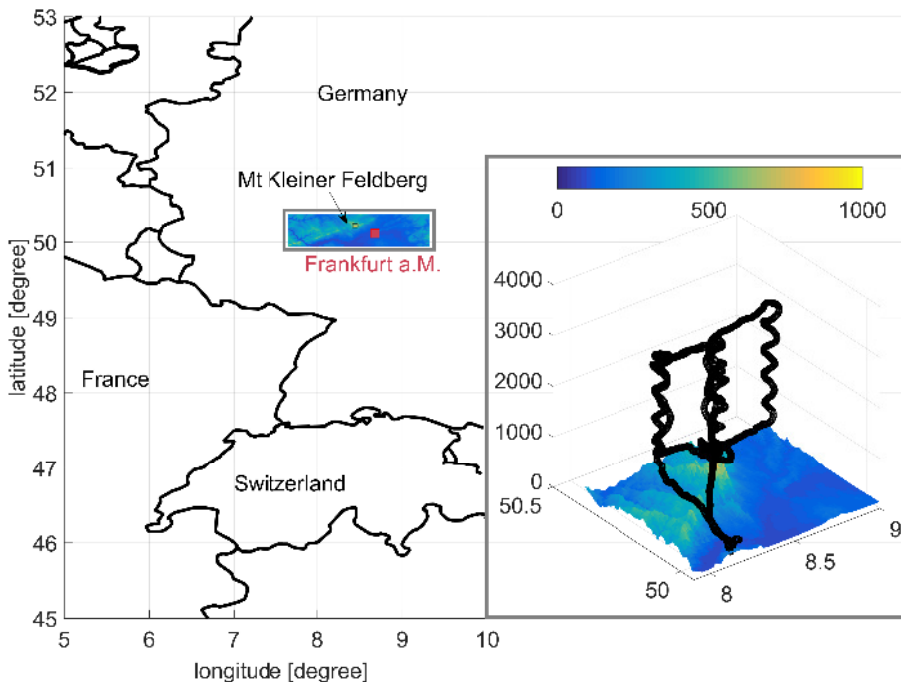
Figure 1. Topographic map (colorbar in m) of the Rhein-Main Area in southwest Germany near Frankfurt am Main including the flight pattern on 6 September 2011 (black line). Vertical profiles are indicated by the flight track spirals. All descending profiles were flown near the summit of Mount Kleiner Feldberg, while ascending profiles have been taken up- and downwind.
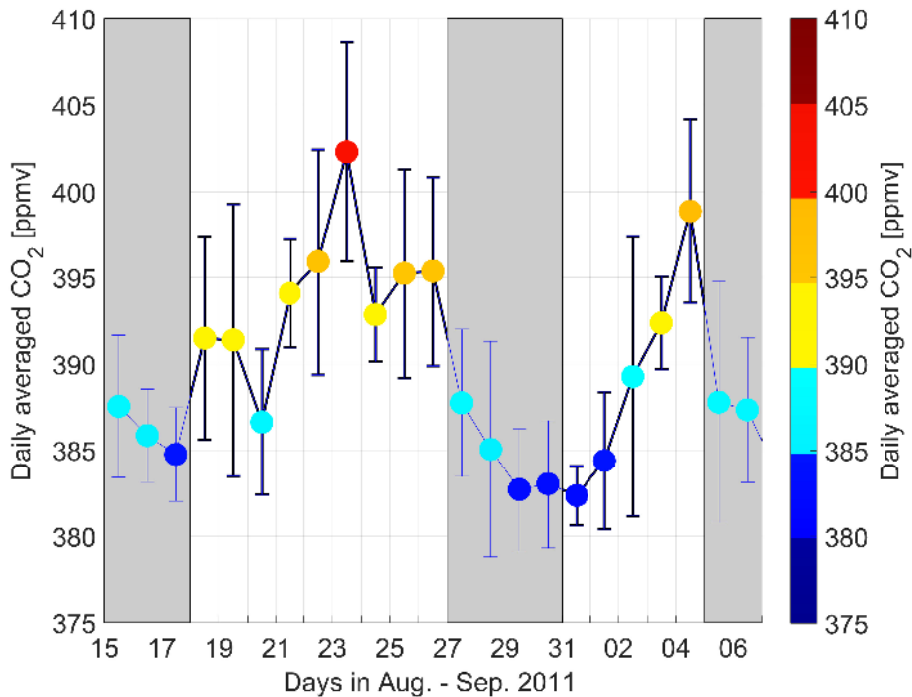
Figure 2. Daily averaged CO_2 observations and the associated standard deviation during the measurement campaign parade on the Mount Kleiner Feldberg. The shaded areas indicate periods of high pressure influence (white) and low pressure influence (gray).
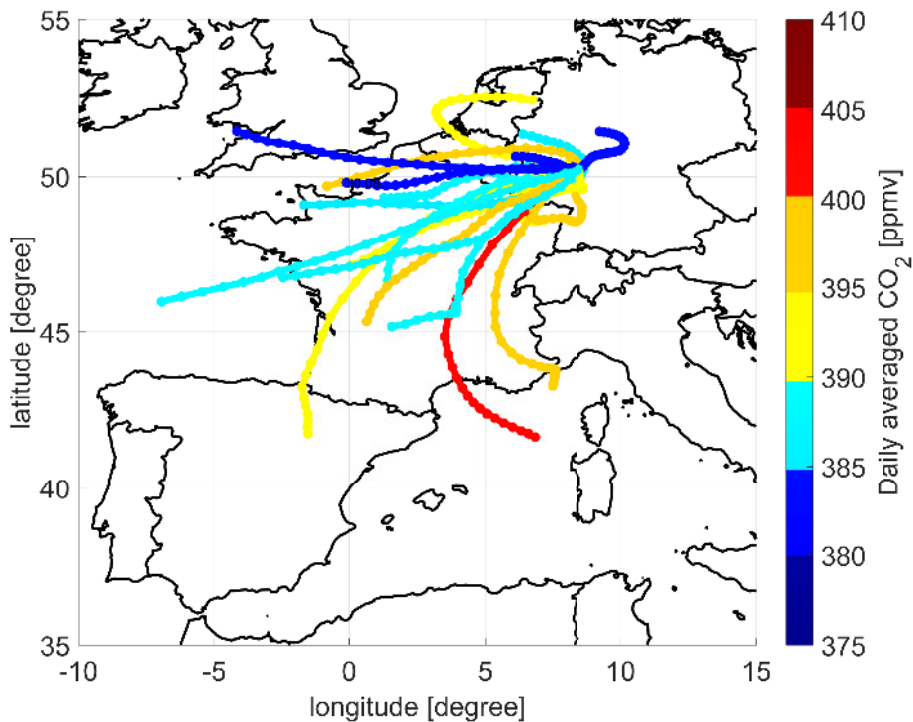
Figure 3. Backward trajectories, starting from the Mount Kleiner Feldberg at 200 m altitude over the surface for each day at 12:00 UTC up to 24 h based by wind fields from COSMO-7. The colors represent the daily averages of CO_2 measurements from Mount Kleiner Feldberg (Fig. 2).
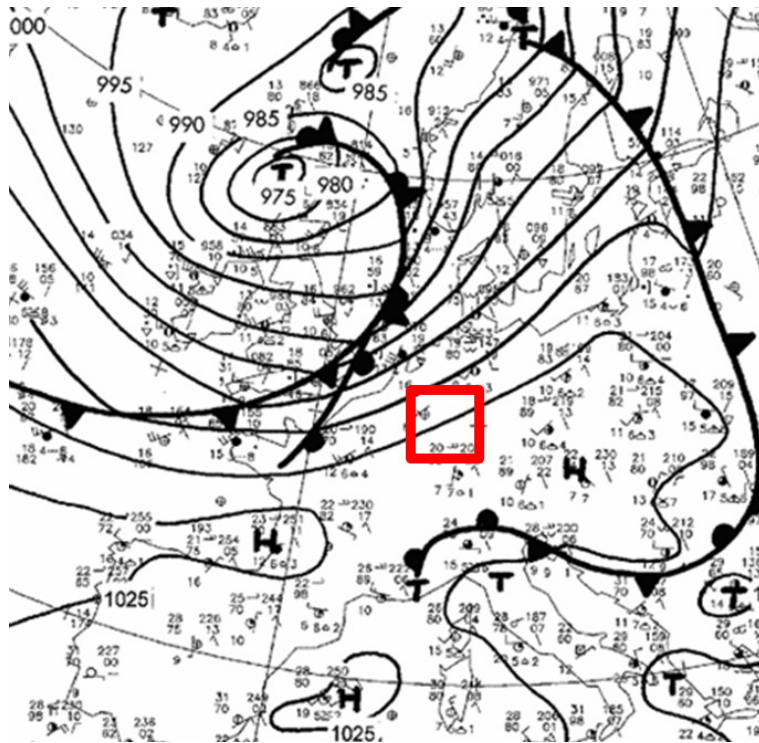
Figure 4. Surface pressure chart provided from the German Weather Service (DWD) over Europe at the 6 September 2011, 12:00 UTC. The red box indicates the measurement area.
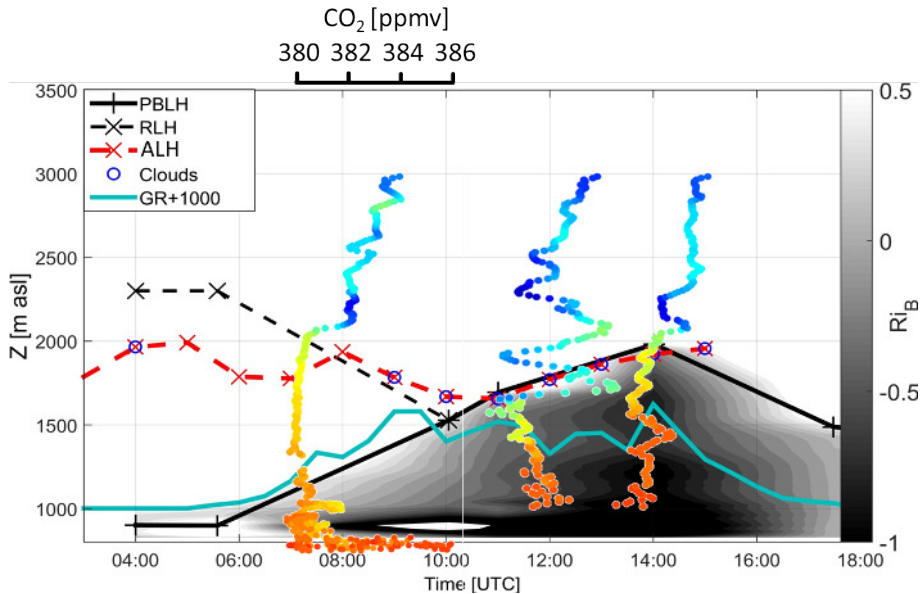
Figure 5. Diurnal variation of the residual layer height (RLH) and planetary boundary layer height (PBLH) derived from radiosondes (black) and ceilometer (red, hourly averaged). The distinction between the turbulent boundary layer and the stable FT is shown by the bulk Richardson number Ri_B (gray scale). RLH is derived from the radiosonde temperature profiles (black dashed) and from one hour averaged aerosol layer heights (AHL) calculated from the ceilometer backscatter profiles (red dashed). Blue circles indicate the occurrence of clouds during that day. The global radiation (GR, blue line) is provided from HLUG in $W\,m^{-2}$. Vertical profiles of CO_2 are shown for different aircraft flights over Mount Kleiner Feldberg during this day in ~~rain bow~~ Rainbow colors, for details see Figs. 7 and 8.
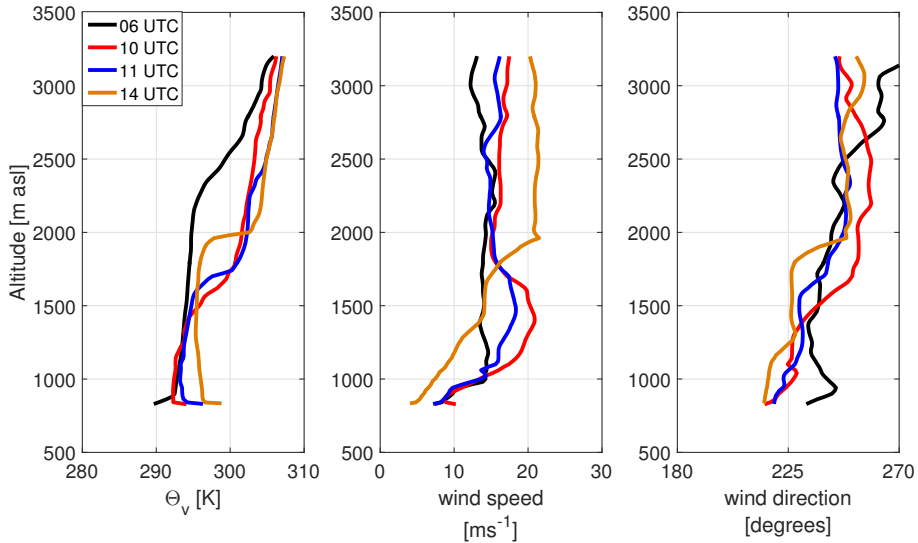
Figure 6. ~~Vertical profiles~~ Profiles of ~~CO₂~~ a) virtual potential temperature, b) wind speed, and ~~of O₃ in the morning (07:27~~ c) ~~.~~ ~~The color shows~~ wind direction derived from radiosondes during the ~~specific humidity. The boundary layer height~~ day (~~dashed~~ black ~~line~~: 6 UTC, red: 10 UTC, blue: 11 UTC, orange: 14 UTC) ~~or residual layer (dashed gray line) height marks the air mass location within the lower atmosphere.~~ on 6 September 2011.
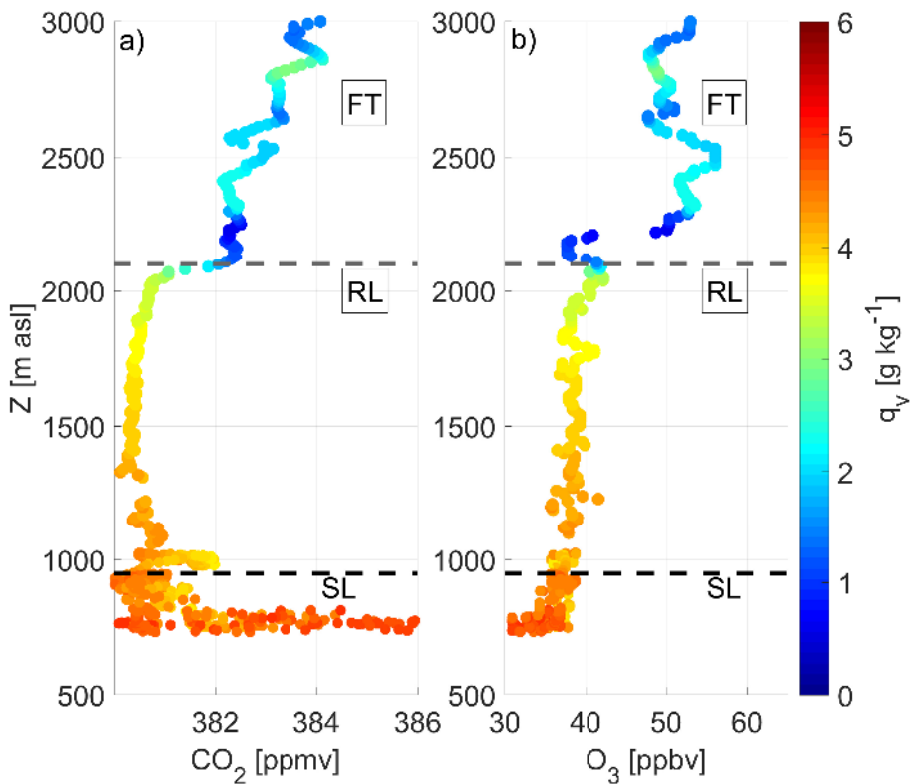
Figure 7. Vertical profiles of a) CO_2 and of b) O_3 in the morning (07:27 UTC) on 6 September 2011. The color shows the specific humidity, and the horizontal lines show the boundary layer height (black dashed line) and the residual layer height (dashed gray line).
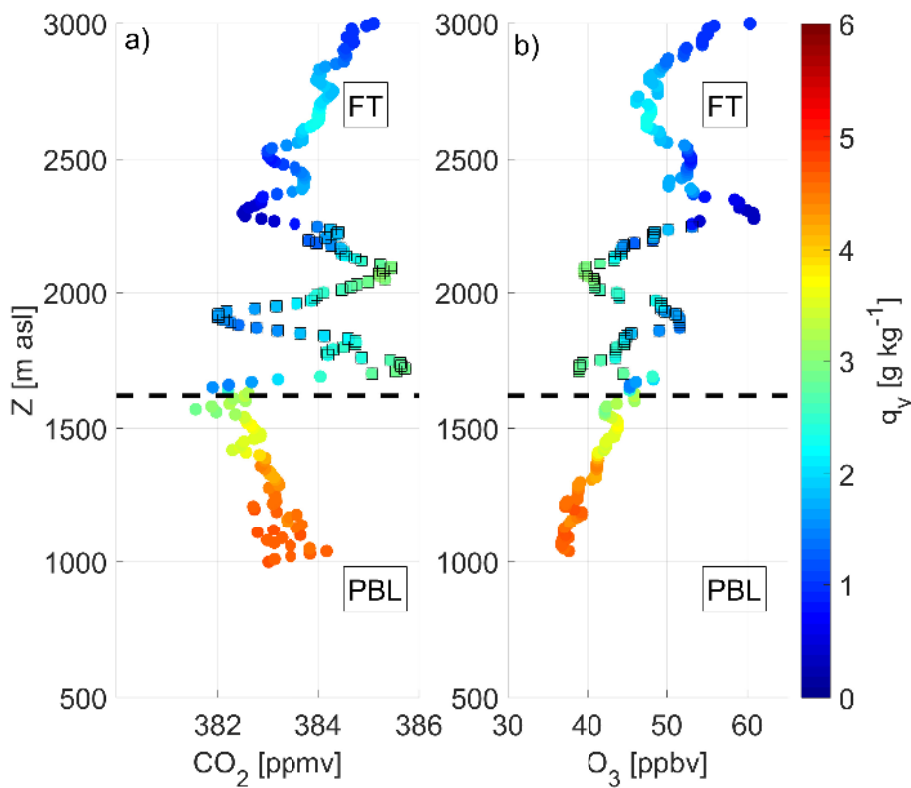
Figure 8. Same as Fig. 7 at noon. The measurement points between 1640 und 2200 m a.s.l. are related due to the mixed air masses influenced by mixing from the SL PBL and the FT.
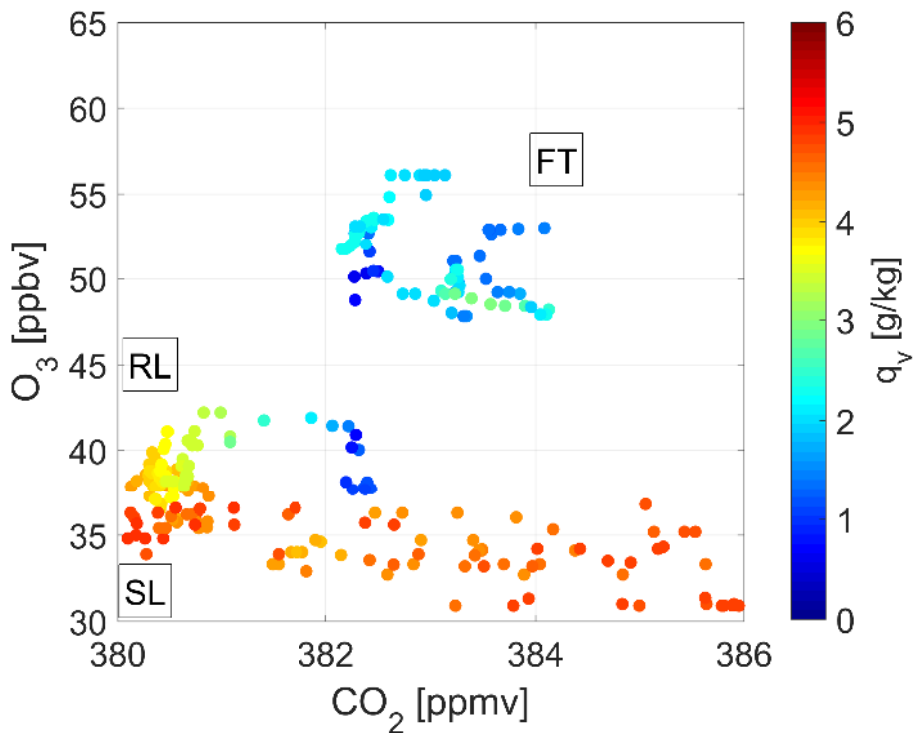
Figure 9. Correlations between CO_2 and O_3 during the observations at ~~11~~07:~~42~~27 UTC color-coded according to specific humidity measurements. The aircraft descended from the FT into the PBL, indicated by a clear separation from the chemical signature.
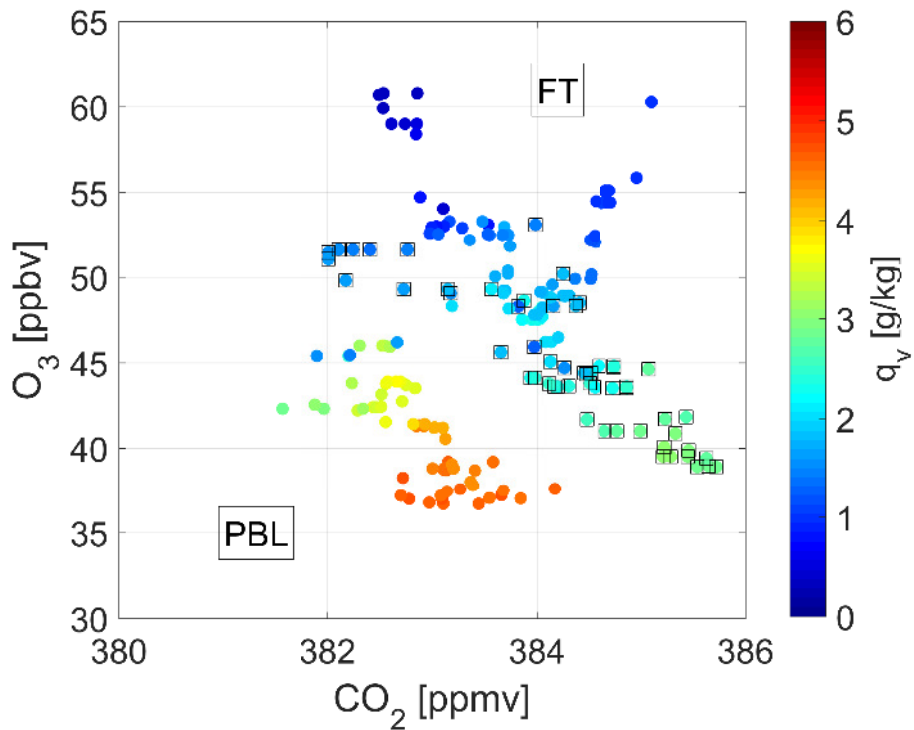
Figure 10. Same as Fig. 9 at noon. The measurement points between 1640 and 2200 m a.s.l. (black boxes) are related due to the mixed air masses from the ~~SL~~ stable Layer and the FT.
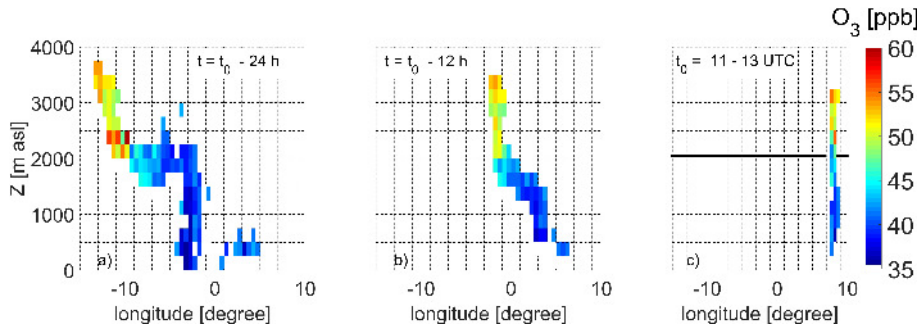
Figure 11. Temporal evolution of air mass origins between 11:00 and 13:00 UTC on 6 September 2011. The trajectory positions are colour coded by mixing ratios of ozone as measured along the flight leg. The data are binned by 0.5° longitude and 250 m altitude (details see text). The black line marks the maximum PBLH during that time.
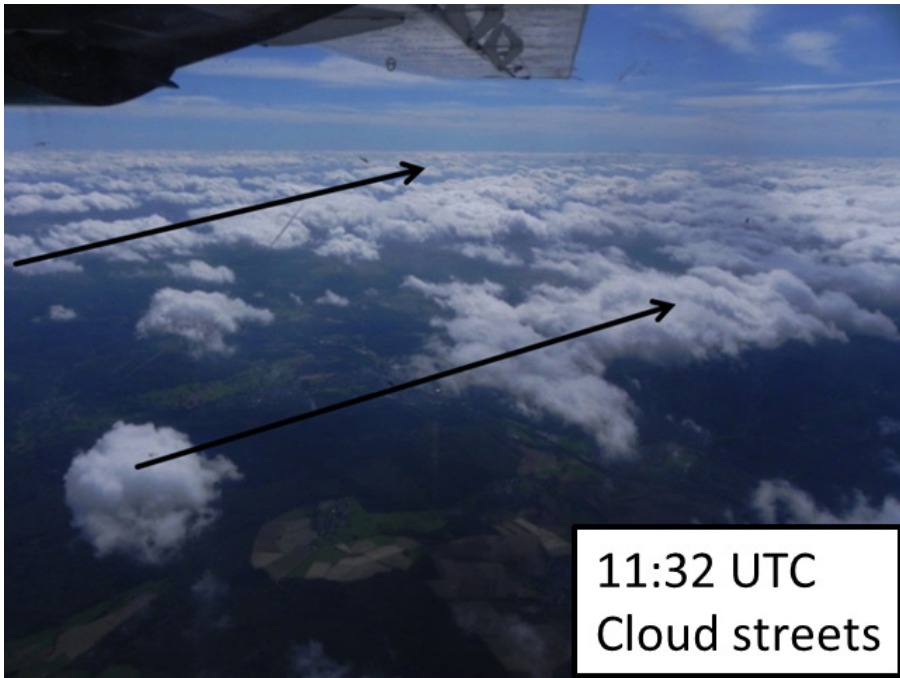
Figure 12. Cloud formation below the flight track at about 11:32 UTC. Just before measuring a profile by descending above Mount Kleiner Feldberg. The arrows shows the mean wind direction.
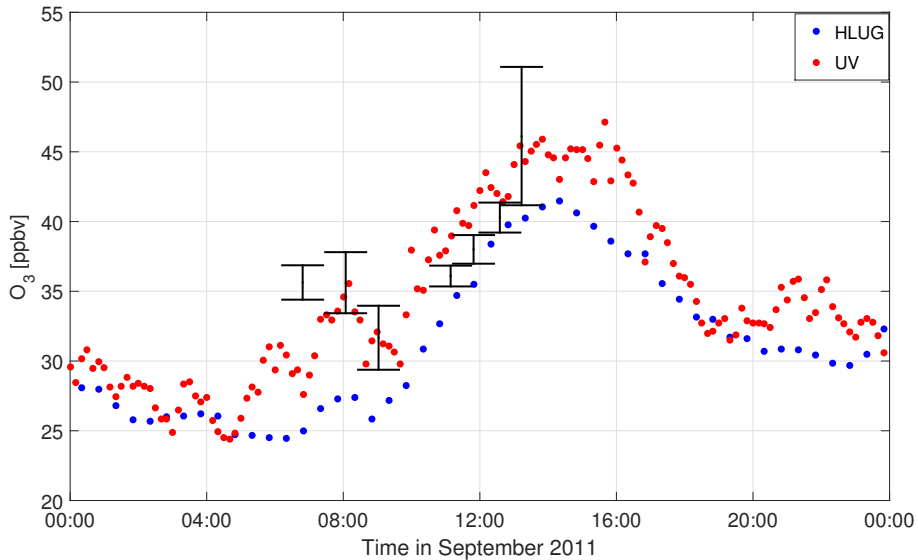
Figure 13. Surface ozone measurements of different instruments at different inlets (HLUG (blue, 30 min-mean) and UV absorption (red, 10 min-mean)) on Mount Kleiner Feldberg (825 m a.s.l.), including the aircraft observations (mean and standard deviation between 1000 to 1600 m a.s.l.) on 6 September 2011.
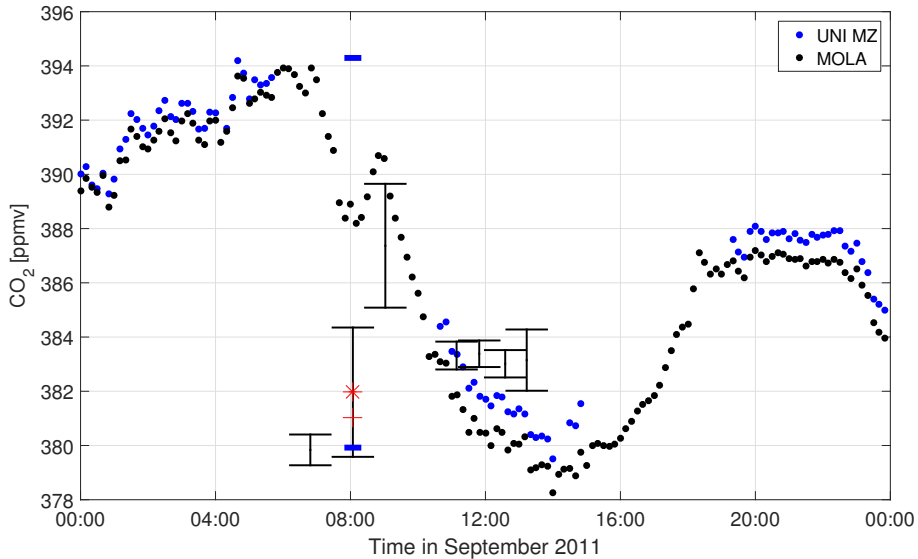
Figure 14. CO_2 surface measurements (on Mount Kleiner Feldberg (825 m a.s.l.), see Sect. 2.2), including the aircraft observations (mean and standard deviation between 1000 to 1600 m a.s.l.) on 6 September 2011. The high CO_2 fluctuations at 08:00 UTC is demonstrated by the mean (red star), standard deviation (black error bars), median (red bar) and maximum/minimum values (blue bar).